Exhumation of basement-cored uplifts: Example of the Kyrgyz Range quantified with apatite fission track thermochronology

Edward R. Sobel,[1] Michael Oskin,[2] Douglas Burbank,[3] and Alexander Mikolaichuk[4]

Received 2 March 2005; revised 30 November 2005; accepted 30 January 2006; published 5 April 2006.

[1] The Kyrgyz Range, the northernmost portion of the Kyrgyzstan Tien Shan, displays topographic evidence for lateral propagation of surface uplift and exhumation. The highest, most deeply dissected segment lies in the center of the range. To the east, topography and relief decrease, and preserved remnants of a Cretaceous regional erosion surface imply minimal amounts of bedrock exhumation. The timing of exhumation of range segments defines the lateral propagation rate of the range-bounding reverse fault and quantifies the time and erosion depth needed to transform a mountain range from a juvenile to a mature morphology. New multicompositional apatite fission track (AFT) data from three transects from the eastern Kyrgyz Range, combined with published AFT data, demonstrate that the range has propagated over 110 km eastward over the last ~7–11 Myr. On the basis of the thermal and topographic evolutionary history, we present a model for a time-varying exhumation rate driven by rock uplift and changes in erodability and the timescale of geomorphic adjustment to surface uplift. Easily eroded, Cenozoic sedimentary rocks overlying resistant basement control early, rapid exhumation and exhibit slow surface uplift rates. As increasing amounts of resistant basement are exposed, exhumation rates decrease while surface uplift rates are sustained or increase, thereby growing topography. As the range becomes high enough to cause ice accumulation and to develop steep river valleys, fluvial and glacial erosion becomes more powerful, and exhumation rates once again increase. Independently determined range-normal shortening rates also varied over time, suggesting a feedback between erosional efficiency and shortening rate. **Citation:** Sobel, E. R., M. Oskin, D. Burbank, and A. Mikolaichuk (2006), Exhumation of basement-cored uplifts: Example of the Kyrgyz Range quantified with apatite fission track thermochronology, *Tectonics*, *25*, TC2008, doi:10.1029/2005TC001809.

1. Introduction

[2] Growth of a contractional mountain range is driven by an evolving relationship between rock uplift, surface uplift, and exhumation [*England and Molnar*, 1990]. In the early phase of orogenesis, rock uplift must outpace exhumation; in a steady state orogen, these reach an equilibrium, while in the final, destructive phase of an orogen, exhumation dominates [e.g., *Willett and Brandon*, 2002]. Temporal changes in key controlling factors, such as fault geometry, shortening rate, and erosion rate will influence the surface uplift history [e.g., *Burbank et al.*, 1996; *Abbott et al.*, 1997; *Stock and Montgomery*, 1999; *Whipple and Tucker*, 1999]. Erosion rate may be controlled by factors such as channel gradients, surface slopes, relief, precipitation, glacial extent, and rock resistance [e.g., *Ahnert*, 1970; *Howard*, 1994; *Brozovic et al.*, 1997; *Hallet et al.*, 1996; *Schmidt and Montgomery*, 1996; *Sklar and Dietrich*, 2001; *Whipple*, 2004]. Because complex interactions among these factors undoubtedly occur, the detailed evolution and interdependence of these factors is rarely delineated.

[3] Reverse-fault-bounded mountain ranges propagating into a foreland basin commonly initiate either as a single, localized structure which gradually lengthens along strike with increasing amount of shortening, or as several fault segments which eventually coalesce or overlap [*Dawers et al.*, 1993; *Cartwright et al.*, 1995; *Davis et al.*, 2005]. In either case, the active range front likely lengthens as displacement accumulates on the range-bounding faults. After several million years of displacement, the original, relatively small structures may be impossible to discern. However, if a reference horizon along the trend of the range exists, range growth and exhumation can be placed into a topographic reference frame by combining low-temperature thermochronologic data with structural geology and geomorphic analysis. When ranges grow through lateral and vertical propagation, spatial trends of exhumation and surface uplift can serve as a proxy for the temporal evolution of the range and permit reconstruction of progressive changes in the balance between rock uplift and erosion [*Burbank et al.*, 1999]. Such space-for-time substitutions are most reliable when time constraints exist for the interval of range propagation. Such along-strike temporal control, however, is commonly lacking in most studies of fold-and-thrust belts. Only when reliable ages can be assigned to various stages of range growth can the validity of the substitution be assessed. We report here a time-

[1]Institut fuer Geowissenschaften, Universitaet Potsdam, Potsdam, Germany.
[2]Department of Geological Sciences, University of North Carolina at Chapel Hill, Chapel Hill, North Carolina, USA.
[3]Department of Earth Sciences, University of California, Santa Barbara, California, USA.
[4]Institute of Geology, Bishkek, Kyrgyzstan.

0278-7407/06/2005TC001809$12.00

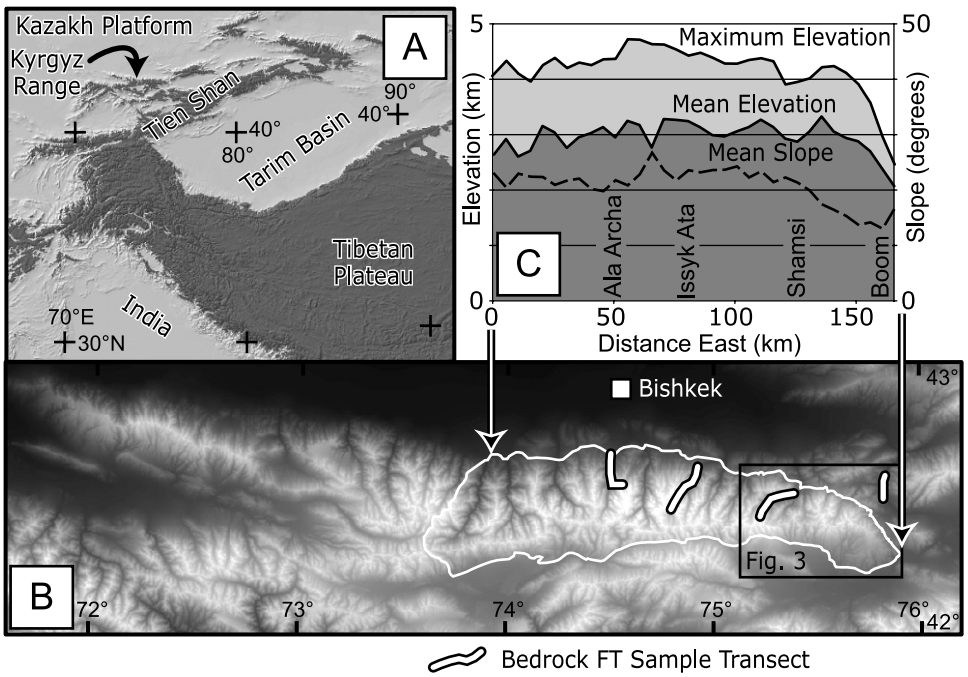

Figure 1. (a) Topographic map of central Asia, showing locations of the Tien Shan with respect to adjacent plateaus and basins. The Kyrgyz Range forms the northern margin of the central Tien Shan. (b) Topography of the Kyrgyz Range derived from 3 arc sec digital elevation model (SRTM). Darker shades correspond to lower topography. Locations of apatite fission track (FT) samples from *Bullen et al.* [2001, 2003] and this study are shown. Irregular outline defines east half of range analyzed in Figures 1c and 4. (c) Mean slope angle, mean elevation, and maximum elevation of the east half of the Kyrgyz Range measured in 10-km-wide swaths. Arrows point to area of analysis of Figure 1b contained within white outline.

calibrated example of range propagation from the Kyrgyz Tien Shan.

[4] The Kyrgyz Range of the northern Tien Shan (Figure 1) provides an example of a reverse-fault-bounded mountain range with topographic evidence for progressive lateral propagation of surface uplift and exhumation. The highest and most deeply dissected sector of the range lies in its central portion, south of Bishkek, in the region of the Ala Archa River. Glaciers mantling peaks up to 4800 m have deeply dissected the granitic range in this region, and young apatite fission track and U-Th/He thermochronometers exhumed from high temperatures indicate >5 km of exhumation at river level [*Bullen et al.*, 2003]. To the east and west, both topography and relief decrease. Moreover, preservation of remnants of a Cretaceous regional unconformity in those areas [*Trofimov et al.*, 1976] implies minimal amounts of bedrock exhumation. If the timing of exhumation of segments of the range outward from the center can be defined, the lateral propagation rate of the range can be estimated and the depth of erosion and time needed to transform a mountain range from a nascent, structurally controlled morphology to a mature, erosionally sculpted morphology can be reconstructed.

[5] Here we present new multicompositional apatite fission track (AFT) data from three transects from the eastern half of the Kyrgyz Range that, when combined with published AFT data, demonstrate that the range has propagated over 110 km from the presently highest region toward the east over the last 7–11 Myr. We synthesize structural data and analyze recently produced digital topography in order to reconstruct the thermal and topographic evolutionary history of the Kyrgyz range. We then present a model for a time-varying exhumation rate driven by the interplay of rock erodability, surface processes, and shortening rate. On the basis of analysis of the digital topography, we discuss whether part of the range has achieved a balance between uplift and erosion and therefore represents a topographic steady state.

2. Geologic History

[6] The Tien Shan records a complex Paleozoic history of island arc accretion [*Burtman*, 1975; *Carroll et al.*, 2001; *Bazhenov et al.*, 2003] followed by Permian strike-slip deformation [*Burtman*, 1975; *Bazhenov et al.*, 1999]. Episodes of intracontinental deformation driven by distal plate margin tectonism occurred during the Early-Middle Jurassic and the Late Jurassic-Cretaceous, documented by foreland basin formation to the north and south of the Tien Shan, as well as in a prominent transtensional basin crosscutting the range [*Hendrix et al.*, 1992; *Sobel*, 1999]. Apatite fission track data suggest pulses of exhumation during the Permian and the Jurassic [*Sobel and Dumitru*, 1997; *Bullen et al.*,

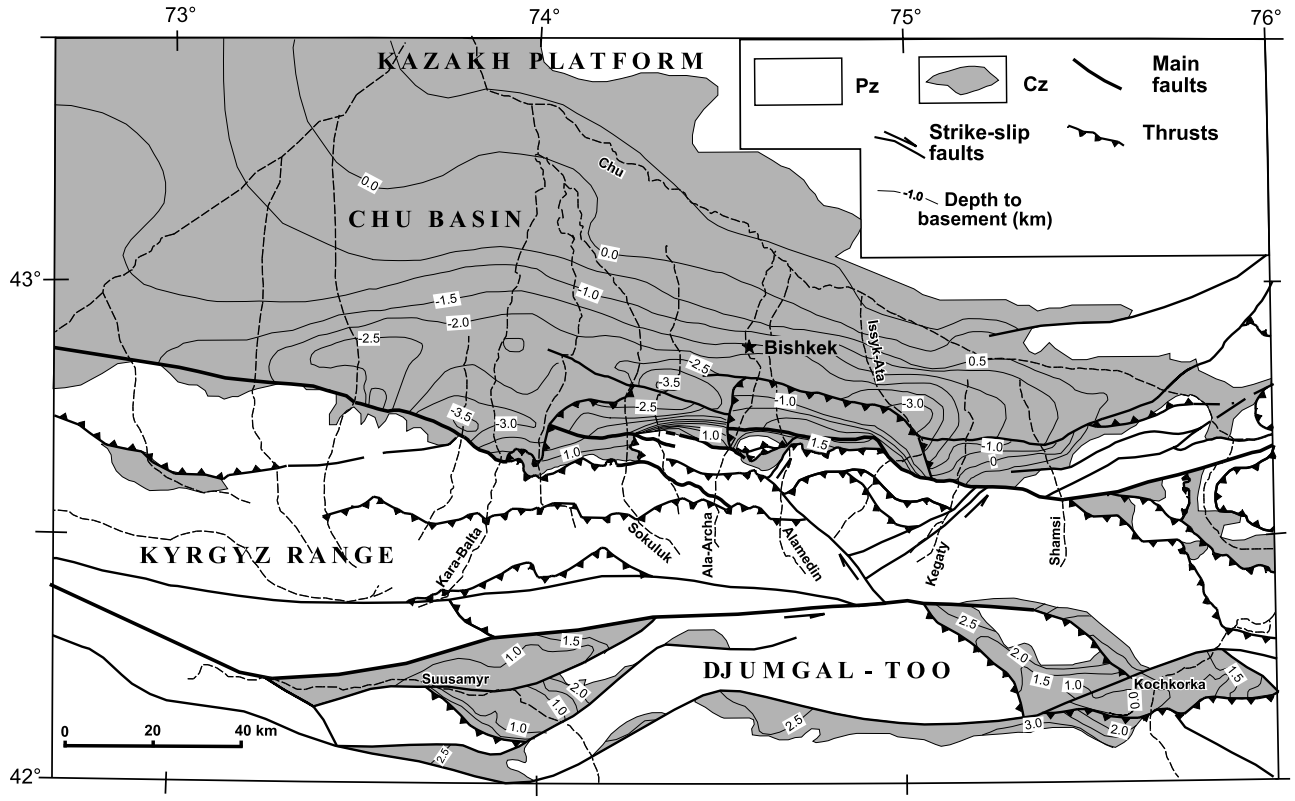

Figure 2. Map of the Kyrgyz range and adjacent basins, modified from *Mikolaichuk et al.* [2003] with permission from the National Academy of Sciences of Kyrgyz Republic. Isopachs show depth to basement; Cenozoic strata of the Chu basin constitute the majority of this sediment. The ranges are composed of Paleozoic units; Mesozoic units are virtually absent.

2001; *Dumitru et al.*, 2001]; these are likely correlated with episodes of deformation within the Tien Shan and deposition within the Tarim basin.

[7] A widespread regional erosion surface formed within the central Kyrgyz Tien Shan in the late Mesozoic [*Trofimov et al.*, 1976; *Makarov*, 1977; *Chediya*, 1986] (see *Burbank et al.* [1999] for photographs). Details of the Mesozoic erosion history are poorly constrained. This surface is unconformably overlain by the Paleocene-Eocene Suluterek formation (also called the Kokturpak formation), containing calcareous sandstone, dolomite, gypsum, and an arid spore-pollen assemblage [*Chediya et al.*, 1973; *Fortuna et al.*, 1994] as well as localized Eocene basalt flows [*Krilov*, 1960]. The formation is typically ~150 m thick and is truncated by an erosional unconformity separating it from upper Tertiary sediments [*Chediya et al.*, 1973; *Fortuna et al.*, 1994]; drilling in the Chu basin reveals that the thickness locally reaches 635 m [*Burg et al.*, 2004]. Overall, this Mesozoic to Tertiary interval of erosion and minor deposition spans ~100 Myr period of tectonic quiescence, during which a stable thermal regime in the upper crust was established [*Bullen et al.*, 2001].

[8] Fission track cooling ages and deposition of apparently syntectonic conglomerates in the adjacent Tarim basin suggest that shortening within the Tien Shan commenced around the Oligocene–Miocene boundary [*Hendrix et al.*, 1994; *Sobel and Dumitru*, 1997; *Yin et al.*, 1998]. This intracontinental deformation is driven by the Eocene – present collision of India with Asia. Deformation within the Tien Shan between 73°E and 80°E longitude (Figure 1) appears to have begun along the southern side of the range adjacent to the Tarim Basin at circa 26 Ma and then propagated northward across the individual ranges of the Tien Shan [*Sobel et al.*, 2000; *Dumitru et al.*, 2001]. Deformation has not propagated monotonically northward; at least the last several million years of this history have been marked by deformation throughout the entire range [*Thompson et al.*, 2002]. At present, seismicity is distributed throughout the width of the orogen [*Bune and Gorshkov*, 1980] and geodetic studies document a continuous gradient of shortening between Kashgar and Bishkek [*Abdrakhmatov et al.*, 1996; *Reigber et al.*, 2001]. Exhumation of the Kyrgyz range on the northern margin of the Tien Shan began in the region of Ala Archa (Figure 2) at ~11 Ma [*Bullen et al.*, 2001]. Deformation is dominantly north vergent thrusting, with a minor sinistral transpressional component [e.g., *Cobbold et al.*, 1996; *Mikolaichuk*, 2000; *Thompson et al.*, 2002] (Figure 2).

[9] The Oligocene-Miocene Shamsi Formation, exposed on the southern margin of the Chu Basin, was deposited in a foreland basin that predated growth of the Kyrgyz Range [*Bullen et al.*, 2001]. The thickness of the pre-11 Ma

sediment in the Chu basin is ~1 km. Although it is difficult to constrain the amount of Cenozoic sediment that formerly overlay the Kyrgyz Range, it may have exceeded the amount in the Chu basin because of flexural subsidence of the predeformational Kyrgyz Range in advance of the northward propagating Tien Shan uplift. This pre-11 Ma burial contributed to the maximum temperature experienced by basement samples during the Neogene. During subsequent exhumation, the weakly lithified Neogene sediment could be more readily eroded than the underlying Paleozoic strata. The Chu basin is deepest in the region of Bishkek and becomes shallower to the east, west, and north [*Abdrakhmatov et al.*, 2001] (Figure 2), suggesting that the magnitude of flexural subsidence and hence the amount of thrusting in the Kyrgyz range is greatest in the central section of the range. *Bullen et al.* [2001, 2003] present a detailed basin and tectonic analysis based on the stratigraphy and magnetostratigraphy of the last ~9 Myr of the Chu basin fill combined both with structural and with apatite U-Th/He and fission track thermochronologic studies of the central Kyrgyz range. This work demonstrates that the range was rapidly exhumed between 11 and 10 Ma along a north vergent thrust; deformation and cooling rates decreased significantly for the next 7 Myr until 3 Ma, when rates increased again. The deformation front propagated slightly between 8 and 3 Ma, coinciding with coarsening upward deposition in the basin. During the last 3 Myr, sediment accumulation rates reached a maximum while the Kyrgyz Range was experiencing rapid rock uplift and exhumation. Concurrently, deformation propagated farther into the foreland, forming a piggyback basin.

3. Geomorphology and Neotectonics

[10] GPS measurements indicate ~20 mm/yr of modern shortening across the central Tien Shan: nearly half of the total convergence rate between India and Asia [*Abdrakhmatov et al.*, 1996; *Reigber et al.*, 2001]. This shortening is distributed across a 400-km-wide belt of subparallel ranges and intramontane basins that are separated by active reverse faults [*Thompson et al.*, 2002]. The Kyrgyz Range forms the northernmost topographic crest within the central Tien Shan. Young thrust fault scarps and seismicity along the northern margin of the range [*Chediya et al.*, 1998; *Thompson et al.*, 2002] attest to ongoing shortening. These ranges form an orographic barrier, with precipitation focused on the northern flanks [*Aizen et al.*, 1995; *Sobel et al.*, 2003].

[11] From a structural perspective, a laterally propagating range would be expected to exhibit increasing amounts of rock uplift and structural relief as a function of distance from the tip toward the center of the range. From a geomorphological perspective, the competition between surface uplift and erosional response [*Kooi and Beaumont*, 1996; *Willett*, 1999] suggests that relief, peak height, hillslope angles, and mean elevation should all initially increase as the range grows. As erosion approaches a balance with rock uplift, relief, mean elevation, and hillslope angles should stabilize. In this study, hillslope angles, topographic relief, and hypsometry were derived from the 3-arc sec digital elevation model (DEM) (Shuttle Radar Topography Mission, SRTM) resampled into Universal Transverse Mercator projection with 70 m pixels. Within 50 km of the eastern tip of the Kyrgyz Range, hillslope angles and both mean and maximum elevation of the Kyrgyz Range all attain average values, supporting our contention that range-scale topographic steady state may prevail over the central part of the range (Figure 1c).

[12] A view of the early stages of geomorphic evolution of the Kyrgyz Range is provided by observations of uplifted and deformed remnants of the pre-Cenozoic erosion surface on its southeastern slope (Figure 3). This exhumed unconformity surface is recognized both in the field and on remote sensing images as concordant, uniformly tilted regions etched by a distinctive dendritic network of shallow bedrock channels [*Oskin and Burbank*, 2005]. On the southern flank of the Kyrgyz Range, southward tilting of remnants of the exhumed unconformity surface increases from east to west (Figure 3), consistent with a model of increasing displacement and range-scale limb rotation above a listric thrust fault [*Erslev*, 1986], such as is proposed to underlie the Kyrgyz Range [*Abdrakhmatov et al.*, 2001]. Field observations at the southern foot of the range and at other nearby outcrops of the erosion surface indicate that it is exhumed from beneath easily eroded Cenozoic continental sedimentary rocks. Remnants of the exhumed unconformity surface can be traced from the foot of the range to the range crest in the easternmost south facing slope of the Kyrgyz Range. Outcrops of the exhumed unconformity surface become increasingly sparse toward the west in response to persistent fluvial erosion and progressively greater range uplift above the Pleistocene glacial equilibrium line altitude (ELA) that promotes corresponding incision of glaciated valleys into bedrock. North facing glaciated valleys also expand laterally via cirque retreat into low-relief south facing erosion surface remnants [*Oskin and Burbank*, 2005]. This process expands the area covered by north flowing glaciers (Figure 3) and shifts the drainage divide southward.

[13] Morphometric analyses of drainage basins that descend from the crest of the Kyrgyz Range link catchment-scale erosion and relief generation to range-scale topographic development. Most of our morphometric analyses focused on the north facing catchments that reach the range crest. Basins were each derived from the DEM with standard hydrologic routing functions, while hypsometry and hillslope angles (Figure 4) were measured directly from the topography and its derivative, respectively.

[14] The distributions of hillslope angle and hypsometry from east to west within the Kyrgyz Range reveal a pattern of initial surface uplift followed by dissection and then stabilization of range-scale morphology. At the easternmost end of the range (surface uplift zone on Figure 4), the mean elevation is <3100 m, peak heights are <4000 m, and the range of hypsometry (measured by difference between the 1st and 3rd quartiles of the hypsometry) is <500 m. Notably, the eastern Kyrgyz Range rises nearly 3 km above the nearby Chu Basin, whereas remnants of Tertiary strata that blanketed the range prior to uplift are now restricted to low elevations on the range flanks. These observations indicate

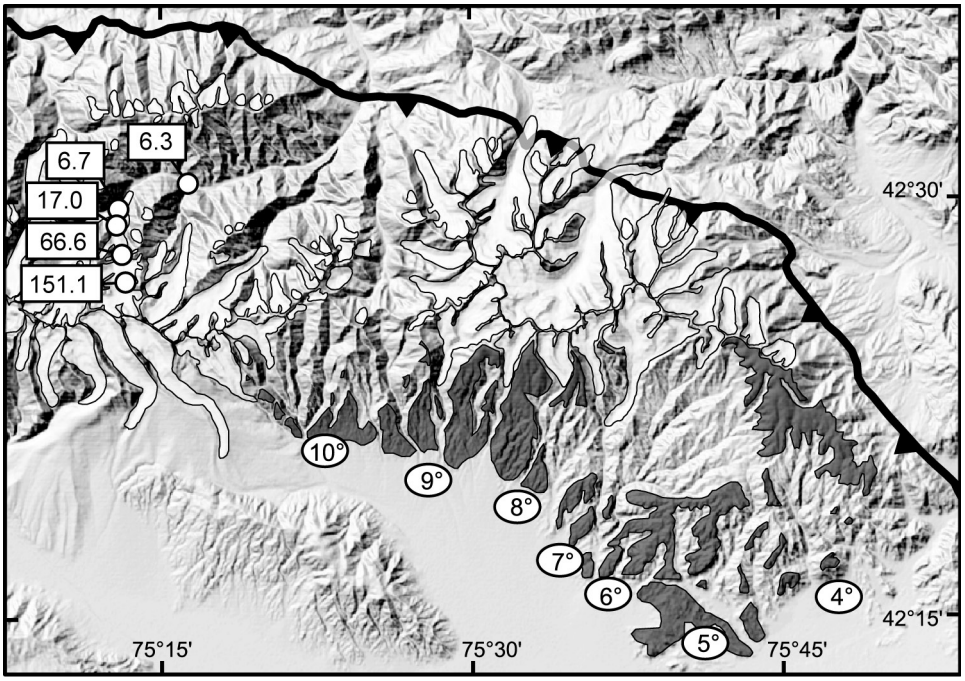

Figure 3. Shaded relief image and map of exhumed pre-Cenozoic unconformity surface remnants of the easternmost Kyrgyz Range. Darker patches are mapped surface remnants with average southward dip shown in degrees. Lighter patches show extent of late Pleistocene glaciation. Reverse fault system bounds northern edge of range. Ages and sample locations from Shamsi River transect show complete exhumation of apatite fission track partial annealing zone northwest of tilted erosion surface outcrops.

that weakly cemented Tertiary strata were readily eroded from the range during rock uplift. In contrast, within the bedrock that constitutes nearly all of the present range, low topographic relief and a restricted range of altitude indicate only limited dissection of this high mountain range and support predominance of surface uplift over erosion here. Moving westward, peak elevations, average hillslope angle, and the range of hypsometry all continue to increase toward the center of the Kyrgyz Range (transition zone on Figure 4), whereas the mean elevation remains nearly constant across this 80-km span. The increase in the elevation of the highest peaks suggests that total rock uplift increases toward the west. Similarly, the increase in the hypsometric range indicate increasing dissection across this tract. In this zone, adjacent basins compete to attain the necessary size, channel gradients, and hillslope angles that permit erosion rapid enough to balance rock uplift. Overall stability of morphologic indices along the central part of the range (steady morphology zone, Figure 4) suggests that this region may have reached an equilibrium topographic form in which erosion balances tectonic uplift. Peak heights, hypsometry, and hillslope angles all begin to decline west of Ala Archa and could indicate erosion and rock uplift rates also decline in this part of the range (Figure 4).

4. Fission Track Methodology

[15] Sample preparation and analytical details are presented in Table 1. The young apatite samples yielded very few horizontal confined track length measurements; up to 100 track lengths were measured from older samples. For age determinations, 15 to 31 grains per sample were selected at random and dated; one sample yielded only four countable grains. Following convention, all statistical uncertainties on pooled ages and mean track lengths are quoted at the $\pm 1\sigma$ level, but $\pm 2\sigma$ uncertainties are taken into account for geologic interpretation. To assess the kinetic properties of apatite, four Dpar measurements were averaged from each dated crystal and from each crystal which yielded a confined track length, provided that sufficient etch pits were present. Dpar values are operator- and etchant-dependent [*Sobel et al.*, 2004]. Therefore seven samples were also analyzed with a CAMECA SX-50 or SX-100 electron microprobe in order to determine Cl content (Table 1). Every crystal with a single grain age or a confined track length measurement was probed. The microprobe data were used to calibrate the Dpar measurements.

[16] Apatite fission track data from exhumed basement rocks often yield distinctive age-elevation patterns that can be used to infer the low-temperature exhumation history of a range. Samples may have been exhumed from sufficient depth during the most recent exhumation event that the maximum temperature, T_{max}, exceeded the total annealing temperature (Figure 5a). In this case, the fission track clock was reset to zero, and fission track data record information on the time-temperature cooling path of the sample as it cooled through the partial annealing zone (PAZ) during exhumation [e.g., *Green et al.*, 1989a, 1989b]. For apatites that are cooled moderately rapidly (10°C/Myr) and which have kinetic parameters similar to Durango apatite, the total

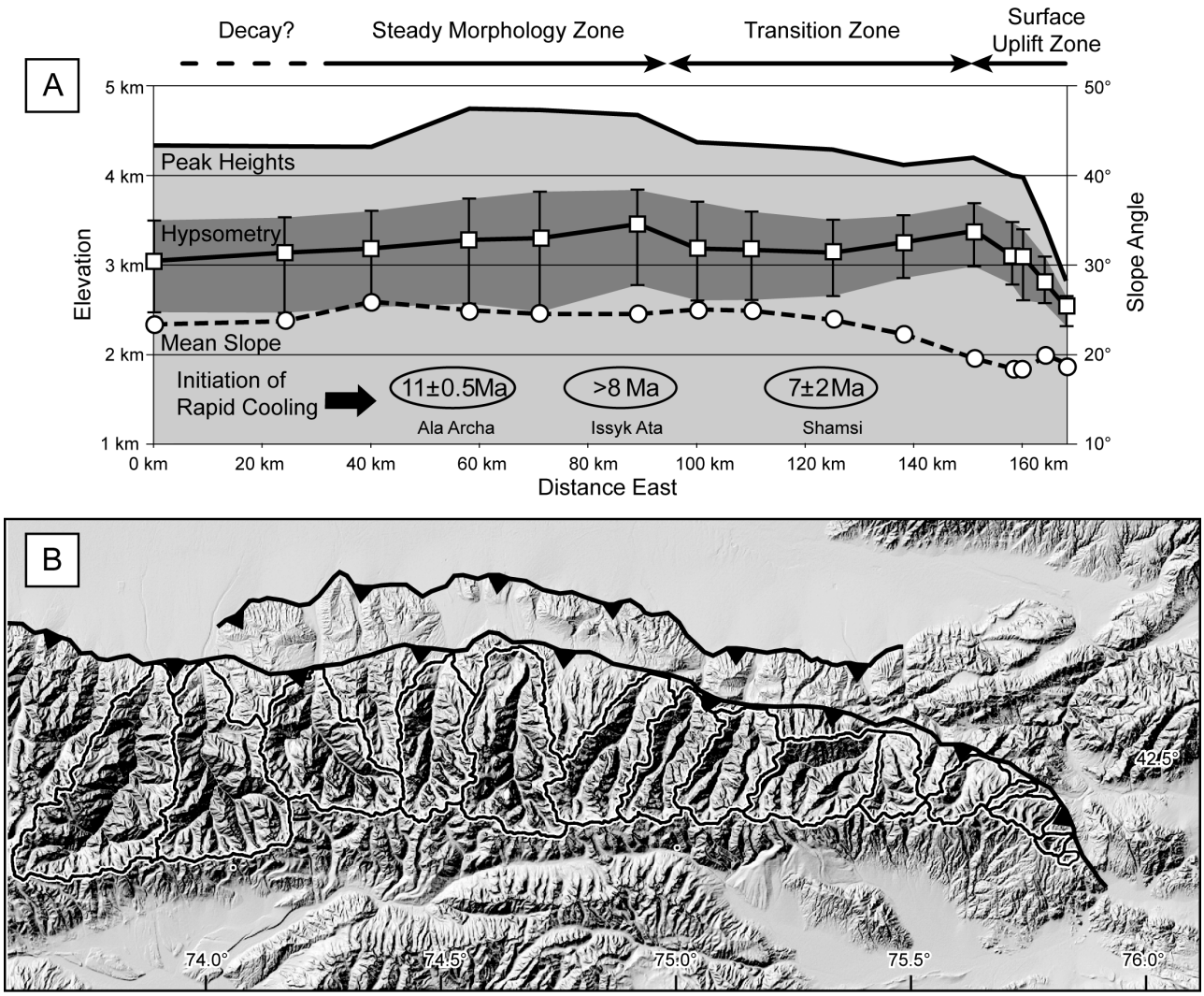

Figure 4. (a) Topographic characteristics of north facing basins along the length of the Kyrgyz range. (b) Measured basins. Peak heights are highest elevations at the edge of each basin. Hypsometry shows median elevation bounded by 75th and 25th percentile elevations. The difference between these is the hypsometric range, shown shaded as medium grey. Surface uplift zone shows sharp increase in peak elevation and hypsometry from east to west in proportion to structural growth of the Kyrgyz Range. Adjustment zone shows progressive increases in mean slope angle and hypsometric range as north facing basins expand and incise uplifted bedrock. These same morphometric indices are constant in the steady morphology zone.

annealing temperature is ~120°C [*Donelick et al.*, 1999; *Ketcham et al.*, 1999]. Samples in the rock column above the total annealing isotherm experienced lower T_{max} prior to exhumation; these samples resided in the (now exhumed) PAZ for some period of time and therefore have ages reflecting the penultimate cooling event, (strongly) modified by partial annealing [e.g., *Fitzgerald et al.*, 1995] (Figure 5a). The age of the transition between these two suites of samples is interpreted to represent the onset of rapid exhumation.

[17] The apatites analyzed in this study often have variable kinetic properties, as documented by both etch pit diameter (Dpar) and Cl content. These two methods have been shown to yield equally useful data for assessing the kinetic properties of apatite [*Donelick et al.*, 1999; *Ketcham et al.*, 1999]. In particular, apatites distinguished by large etch pit diameters and high Cl content (herein termed "more resistant") are typified by higher annealing temperatures in contrast to less resistant apatites [e.g., *Green et al.*, 1989b; *Ketcham et al.*, 1999]. Apatites analyzed in this study exhibit 10–15°C of variability in total annealing temperature. Given these contrasting annealing temperatures, a superficial interpretation of an age-elevation plot can yield false conclusions about both the onset and rate of exhumation. Although the total annealing temperature of different apatite types is variable, the low-temperature annealing behavior of apatites appears to be similar [*Ketcham et al.*, 1999; *Crowhurst et al.*, 2002].

Table 1. Fission Track Data From the Kyrgyz Range[a]

Sample	Irradiation Code	Component	Age	Lithology	Lat N	Long E	Altitude (GPS), m	Altimeter, m	Xl[b]	Rho-S,[c] $\times 10^5$	NS[d] §	Rho-I,[c] $\times 10^5$	NI[d] §	P(χ^2),[e] %	Rho-D,[f] $\times 10^6$	ND[g]	Age, Ma	±1σ Error	U, ppm	Dpar, μm	SD, μm	Cl, wt %	Length, μm	Error, μm	SD, μm	Number of Lengths
														Issyk Ata											
TS161	UP32-13+		O3	granite	42°30.108	74°52.901	3350	3290	31	1.9880	145	11.750	857	0	1.3330	5420	24.5	7.6	11.0	1.85	0.29	0.10	12.92	0.32	1.63	26
	UP43-6+	young							25	0.3097	17	10.040	551	93	1.3330	5420	7.6	1.9	9.4	1.72	0.16	0.02				
	UP43-7	old							6	7.0970	128	16.980	306	0	1.3330	5420	102.0	11.0	15.9	2.13	0.34	0.17				
TS159	UP32-12		O3	granite	42°31.108	74°52.425	na	2850	20	1.0280	132	33.790	4338	8	1.2330	5034	6.9	0.6	34.3	1.87	0.14		13.50	0.49	1.37	8
TS158	UP32-11		O3	granite	42°32.364	74°52.178	2560	2560	25	0.5357	47	25.620	2248	99	1.2260	5034	4.7	0.7	26.1	1.36	0.09	0.02				0
TS162	UP43-8		O3	granite	42°33.391	74°53.351	2380	2350	31	0.4456	59	24.740	3275	24	1.3240	5420	4.4	0.6	23.4	1.92	0.08		13.44	0.07	0.10	2
TS163	UP43-9		R	metavolc	42°34.854	74°54.187	2060	2090	4	0.4827	4	21.600	179	74	1.3140	5420	5.4	2.8	20.5	1.84	0.35					0
Mav38	UP65-10+11		O3	granite	42°37.912	74°55.100	1840		34	0.2850	34	1.480	1765	93	1.0847	4531	3.9	0.7	17	1.65	0.25					
														Shamsi											
TS170	UP32-16		C2-3	sandstone	42°27.344	75°14.024	3865	3770	22	4.814	636	12.120	1601	4	1.2580	5034	91.1	5.6	12.0	1.65	0.13	0.12	12.58	0.33	1.53	22
TS169	UP32-15		C1	sandstone	42°27.751	75°13.944	3697	3570	19	16.2100	836	24.530	1265	22	1.2520	5034	151.1	7.7	24.5	2.04	0.16	0.26	12.06	0.17	1.69	100
TS167	UP43-12		C1	sandstone	42°28.237	75°13.135	3254	3160	24	4.0790	661	14.470	2344	18	1.2850	5420	66.6	3.4	14.1	1.96	0.14	0.10	11.89	0.26	1.88	52
TS166	UP32-14		C1	sandstone	42°29.301	75°12.973	2930	2870	22	1.0780	146	13.930	1886	35	1.2450	5034	17.0	2.0	14.0	1.74	0.15		14.38	0.47	0.95	4
TS165	UP43-11		C1	sandstone	42°29.830	75°12.996	2670	2610	12	0.6100	27	12.700	562	0	1.2950	5420	13.7	7.0	12.3	1.80	0.21	0.12	12.95			1
		young							11	0.3629	15	13.040	539	62	1.2950	5420	6.7	1.8	12.6	1.74	0.17	0.12				
		old							1	4.1030	12	7.864	23	na	1.2950	5420	123.6	44.1	7.6	2.04	na	0.11				
TS164	UP43-10		C1	sandstone	42°30.739	75°16.158	2280	2250	20	0.3551	63	13.590	2412	85	1.3040	5420	6.3	0.8	13.0	1.74	0.11	0.07	11.99	0.97	2.57	7
														Boom Gorge											
TS84	UP30-17		P	granite	42°32.688	75°48.867	1530	1620	20	9.694	826	15.410	1313	84	1.3070	5224	150.2	7.6	14.7	1.70	0.11		12.50	0.23	1.99	73
TS27	UP2-20		D-C3	sandstone	42°38.010	75°50.562	1376	na	12	6.378	569	9.394	838	12	1.0510	4299	127.5	10.1	11.2	na	na		12.82	0.20	1.96	100

[a]Sample preparation and analysis were similar to that outlined by *Sobel and Strecker* [2003]. Samples analyzed with a Leica DMRM microscope with drawing tube located above a digitizing tablet and a Kinetek computer-controlled stage driven by the FTStage program [*Dumitru*, 1993]. Analysis performed with reflected and transmitted light at 1250X magnification. Samples were irradiated at Oregon State University, except TS27, which was irradiated at Risø National Laboratory, Denmark. Following irradiation, the mica external detectors were etched with 21°C, 40% hydrofluoric acid for 45 min. The pooled age (central age) is reported for samples with P(χ^2) greater than (less than) 5% as they pass (fail) the $\chi 2$ test; error is one sigma, calculated using the zeta calibration method [*Hurford and Green*, 1983] with zeta of 369.6 ± 7.6 for apatite (E. Sobel, unpublished data, 2003). Sample TS27 calculated with a zeta of 361 ± 20 (E. Sobel, unpublished). Note that three slides were combined for sample TS161 and two for Mav38.

[b]Xls is the number of individual crystals dated.

[c]Rho-S and Rho-I are the spontaneous and induced track density measured, respectively (tracks/cm^2).

[d]NS and NI are the number of spontaneous and induced tracks counted, respectively.

[e]P(χ)^2 (%) is the chi-square probability [*Galbraith*, 1981; *Green*, 1981].

[f]Rho-D is the induced track density in external detector adjacent to CN5 dosimetry glass (tracks/cm^2).

[g]ND is the number of tracks counted in determining Rho-D. Microprobe measurements were performed with PAP correction procedures, operating conditions of 15 kV beam, beam current of 20 nA (measured on a Faraday cup) and a ~15 μm beam diameter. Chlorine was measured for 100 s, providing a ~150 ppm detection limit. Calibration included a Durango apatite standard which was repeatedly measured during the course of analysis.

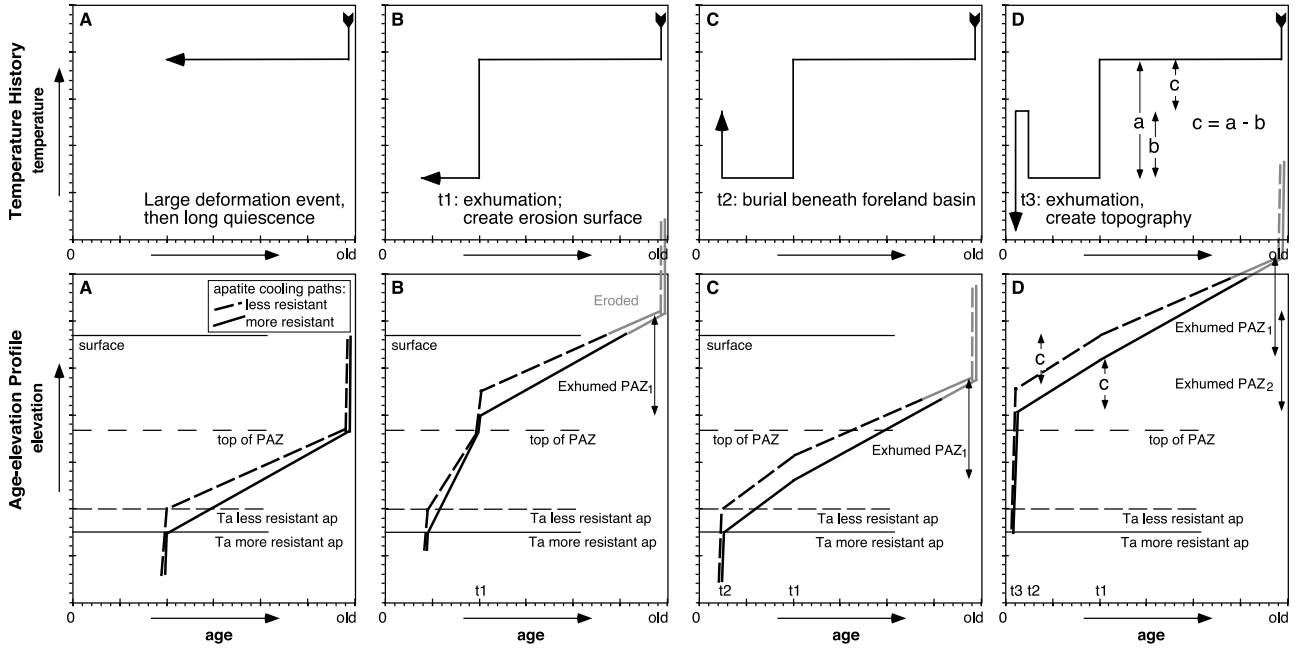

Figure 5. Schematic illustration of the affect of differing total annealing temperatures (T_a) on complex cooling paths. The four vertical elevation profiles represent a sequence of exhumation (cooling) and burial (reheating) events. (top) Evolving temperature history and (bottom) distribution of apatite fission track ages in a vertical profile at the corresponding time step. Each profile shows the cooling path of apatites that are more (solid line) and less (dashed line) resistant to annealing. The base of the partial annealing zone (PAZ) for each type of apatite is considered to be the respective T_a. Exhumation and burial events are (unrealistically) depicted as instantaneous for clarity. The geothermal gradient is assumed to remain constant and advection of isotherms is neglected for simplicity. (a) A large deformation event followed by a long period of quiescence gives shallow samples a common age. More resistant apatites are reset at lower elevation (hotter temperature); therefore the slope of the more resistant cooling path is steeper in the PAZ. (b) Large exhumation event at time t_1 forms exhumed PAZ_1. A new PAZ forms at depth. (c) Section buried and reheated beneath sediments of a sedimentary basin at time t_2. Heating resets all apatites below their respective T_a. Exhumed PAZ_1 is partially reset. In the lower part of the current PAZ, cooling paths for apatites with different T_a may be parallel. If the exhumation event was large enough to shift the entire PAZ_1 to a temperature hotter than the appropriate T_a, then the exhumed PAZ_1 would be completely overprinted. (d) A second large exhumation event that creates new exhumed PAZ_2 at time t_3. Ongoing exhumation could subsequently expose the entire exhumed PAZ in mountainous topography. If the simplifying thermal assumptions are correct, the shape of the age-elevation curve can be used to reconstruct the magnitude of thermal events. The difference between the magnitude of exhumation t_1 (Figure 5a) and burial (Figure 5b) is equal to the difference between the base of PAZ_1 and the base of PAZ_2 (Figure 5c) (for a given apatite type). Therefore, if the base of PAZ_1 and PAZ_2 can be determined and the magnitude of burial can be constrained by thermal modeling or independent geological data, it is possible to estimate the magnitude of exhumation that occurred at t_1.

Therefore the slope of the exhumed partial annealing zone on an age-elevation plot for different apatite types cannot be assumed to be parallel (Figure 5). To avoid this pitfall, we have plotted age-elevation curves for apatites with similar kinetic properties. The long period of tectonic quiescence prior to the onset of Neogene exhumation implies a stable thermal structure in the upper crust [*Bullen et al.*, 2001]. Therefore the slope of the age-elevation curve within the exhumed PAZ for kinetically similar apatites which have experienced similar thermal histories should be about the same for all of our profiles. This assumes that only a small, similar amount of horizontal axis rotation has been experienced at each of the profiles located in the hanging wall of a major thrust. A contrasting age-elevation slope will pertain for apatites with differing kinetic characteristics (see Figure 5). We utilize the AFT data from three transects to reconstruct the onset and rate of exhumation for each transect. Subsequently, Cenozoic burial and exhumation histories are evaluated using thermal models of higher elevation samples.

5. Results

5.1. Shamsi

[18] Samples were collected along a tributary of the Shamsi river valley between 2250 and 3770 m along a

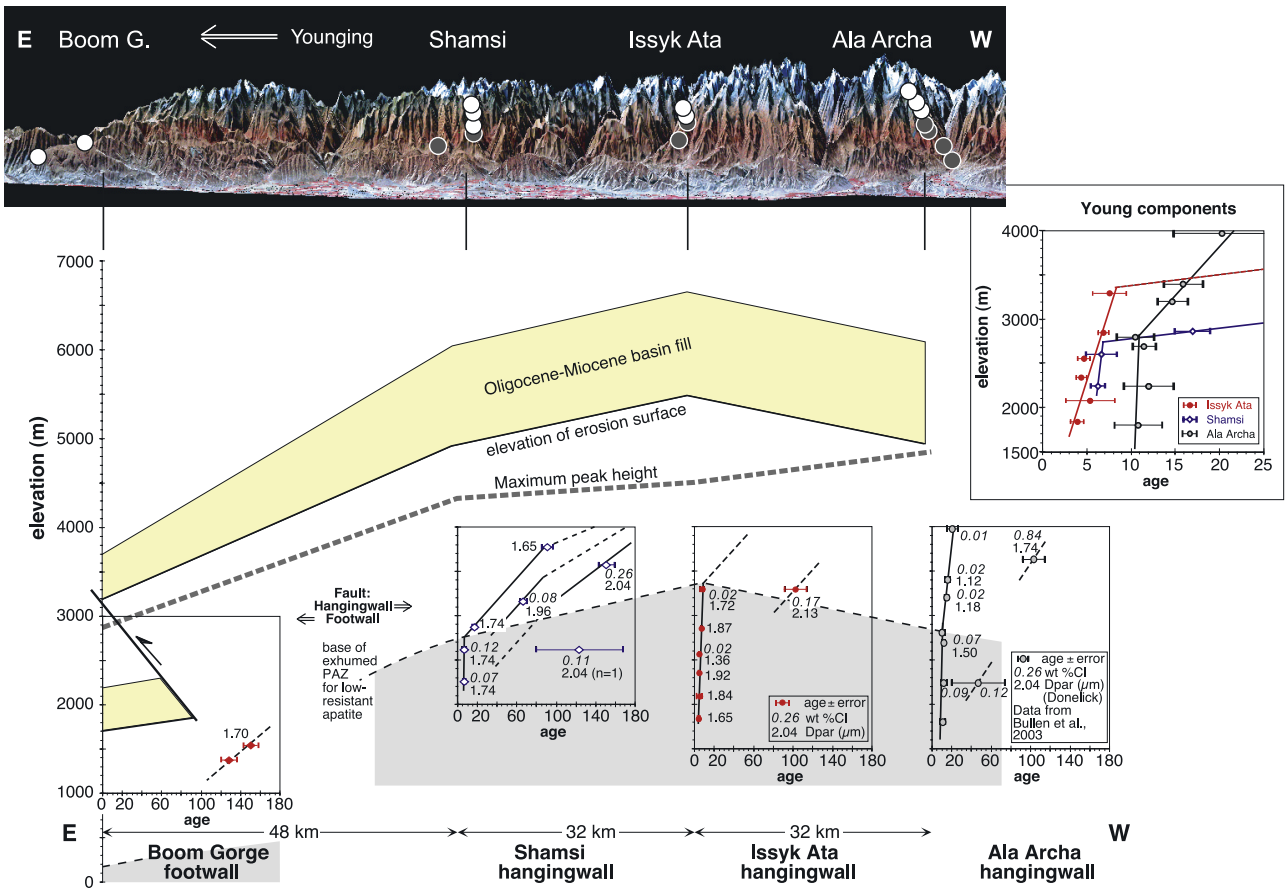

Figure 6. Fission track age plotted versus elevation for the Boom Gorge, Shamsi, Issyk Ata, and Ala Archa sections (from left to right; east to west). All samples are plotted on a common vertical axis. Boom Gorge is in the footwall; other sections are in the hanging wall. Inset at top right shows the young portion of the three hanging wall sections. Numbers next to samples indicate kinetic character of apatite; italics denote wt % Cl; normal text denotes Dpar. Ala Archa data is from *Bullen et al.* [2003]; Dpar values from this profile are not directly comparable with other Dpar values shown as Dpar measurements depend on both the operator and the etching conditions [*Sobel et al.*, 2004]. Top dashed line indicates the maximum peak elevation. Bottom dashed line indicates position of base of exhumed PAZ for low-chlorine apatite. Fine dashed line shows approximate age-elevation path, constructed following Figure 5. Amount of exhumation calculated using a geothermal gradient of 26°C/km [*Gubin*, 1986] and the T_a (Table 2). Thermal conductivity of young sediments and basement were not differentiated. Grey region indicates average thickness of sedimentary basin that could have formerly overlain the range; the upper and lower limits are ±∼300 m. The image at the top shows a multispectral scanner image draped over an SRTM DEM, depicting the view of the range looking from the north. Grey scale image is composite brightness of visible and near-infrared bands of Landsat 3 multispectral scanner (MSS) bands 2, 3, and 4. White circles denote the location of partially reset fission track samples; grey circles denote fully reset samples.

transect that traverses a continuous sequence of Carboniferous sandstone from the base of the valley up to the crest of the east flanking ridge (Figure 3).

[19] The six samples yielded Miocene to Jurassic ages, generally increasing with elevation (Table 1 and Figure 6). Four define a readily interpretable succession that captures the base of an exhumed partial annealing zone. These samples also illustrate the complications introduced by apparent mixtures of apatites with different annealing temperatures within the same bedrock sample. With an age of 6.3 ± 0.8 Ma, the basal, youngest sample (TS164) passes the χ^2 test; all analyzed grains have similar kinetic properties as shown by Dpar (1.74 μm, SD 0.11) and microprobe (0.07 wt % Cl, SD 0.05) (Table 1 and Figures S1–S6 in the auxiliary material).[1] The next sample (TS165) has a central age of 14 ± 7 Ma and fails the χ^2 test. Eleven of the twelve countable grains form a young population, pass the χ^2 test with a pooled age of 6.7 ± 1.8 Ma and a mean Dpar of 1.74 μm. A single grain has an age of 124 ±

[1]Auxiliary material is available at ftp://ftp.agu.org/apend/tc/2005tc001809.

44 Ma and a Dpar of 2.04 μm. However, microprobe data does not differentiate this grain; the average chlorine value of the sample is 0.12 wt % and the old grain has a value of 0.11 wt %. This illustrates that chlorine is not the only factor affecting resistance to annealing. The third sample (TS166) passes the χ^2 test and has a pooled age of 17 ± 2 Ma and a Dpar value of 1.74 μm. The highest elevation sample (TS170) fails the χ^2 test and has a central age of 91 ± 6 Ma, a Dpar value of 1.65 μm, and 0.12 wt % Cl. However, one crystal has an anomalously high wt % Cl of 0.45% and an age of 114 ± 13 Ma; excluding this grain, the sample passes the χ^2 test and has a pooled age of 88 ± 5 Ma and 0.07 wt % Cl. For these latter two samples, there is no relationship between age and Dpar. Excluding the single old, high Dpar grain in sample TS165, these four samples can be plotted together on an age-elevation plot (Figure 6).

[20] The lower two samples show rapid cooling, while the upper two show slow cooling within an exhumed PAZ. The inflection point between the two segments, at ~2800 m and 7 ± 2 Ma, defines the onset of rapid cooling. Assuming that the sample experienced some amount of heating due to Miocene sedimentation and related burial prior to rapid exhumation, the total annealing temperature corresponding to the inflection point of this low Cl path is 100–105°C. On the basis of the age and elevation differences of these two partially reset samples, the slope of the exhumed PAZ is about 12 ± 1 m/Myr (0.012 ± 0.001 km/Myr). This value will be used to define the slope of the exhumed PAZ at Issyk Ata because this section experienced a similar burial history (compare Figure 5). As will be shown below, the corresponding slope at Boom Gorge is ~0.01 km/Myr, supporting this assumption. After 7 Ma, the rate at Shamsi accelerated to ~1 km/Myr.

[21] Two additional samples lie within the exhumed PAZ. Both pass the chi-square test. TS167 has an age of 67 ± 3 Ma, Dpar of 1.96 μm and 0.10 wt % Cl (0.08 wt % Cl excluding five grains with high values); TS169 has an age of 151 ± 6 Ma, Dpar of 2.04 and 0.26 wt % Cl (Table 1 and Figures S1–S6). Because TS169 is significantly older than the two bounding samples TS167 and TS170, plotting all of the samples within the exhumed PAZ together cannot yield a readily interpretable age-elevation plot. However, placing kinetically different samples on subparallel trends reveals that more resistant apatites have consistently older ages, representing older portions of an exhumed PAZ.

5.2. Issyk Ata

[22] Samples were collected from a transect along the Issyk Ata river valley between 1840 and 3290 m (Figure 4). Nearby, glaciated peaks reach elevations of 4500 m. The samples are primarily from Late Ordovician granite; the second sample above the base of the transect is an apatite-poor Riphean metavolcanic rock.

[23] Five of the six analyzed samples pass the chi-square test, yielding ages ranging from 3.9 ± 0.7 Ma to 6.9 ± 0.6 Ma (Table 1 and Figure 6). Four of these samples, Mav38, TS158, TS159, and TS162 appear to be monocompositional based on Dpar measurements and microprobe analysis. Dpar values are 1.65, 1.36, 1.87, and 1.92, respectively; the second of these sample yields a wt % Cl of 0.02 (Table 1 and Figures S1–S6). Sample TS163 yielded only four countable grains; the resulting age is consistent with the other samples but of too low precision to warrant further attention. Sample TS161 contains two components that each pass the chi-square test. A young population of 25 grains yields an age of 7.6 ± 1.9 Ma; an older component with six grains provides an age of 102 ± 11 Ma. The younger population has a Dpar of 1.72 μm and a wt % Cl of 0.02. Kinetic characteristics do not explain all of the grains in the older population: five of the six older grains yield higher values of 0.17 wt % Cl, whereas one grain has a value of 0.01 wt % Cl. Three of the old grains have large Dpar values of 2.43; the other three fall within the cluster of young grains with an average value 1.83. When combined, the six grains have an average value of 2.13 μm.

[24] The young, low resistant grains from these six samples define a steep linear trend on an age-elevation plot, indicating rapid cooling from below the base of an exhumed PAZ. The trend of the corresponding exhumed PAZ is assumed to have the same slope as the corresponding curve at Shamsi. Because of the absence of low resistance, partially reset samples, the position of this latter curve is poorly defined; hence the onset of this rapid cooling can only be constrained as older than about 8 Ma. Using Figure 5d as an analogy, the slope of the exhumed PAZ through the more resistant component of sample TS161 should have the same slope as the less resistant component; the two curves should be separated by a vertical distance corresponding to the difference in T_a for the two components. Although the more resistant slope is poorly constrained, this analysis suggests that the onset of rapid cooling should be represented by an elevation close to TS161 and hence only slightly older than 8 Ma.

5.3. Boom Gorge

[25] Two samples were collected from the Boom Gorge along the Chu River at 1375 and 1530 m; these lie ~1500 m below the local peaks (Figure 4). Both samples are from topographically low positions in the footwall of the main range-bounding thrust, in contrast to the hanging wall sections sampled at Shamsi and Issyk Ata. Cenozoic sediments lying above the regional erosion surface are preserved in the center of the range, where they are overthrust by Paleozoic strata. The same sedimentary sequence lies north and south of the range, overthrust from the south and north, respectively. The Cenozoic strata in this region do not exceed 1.5 km in thickness [*Trofimov et al.*, 1976]. Sample TS84 was collected from a Permian granite just below the unconformity surface. Sample TS27 was collected from Devonian–Upper Carboniferous sandstone.

[26] The two samples both pass the chi-square test, with pooled ages of 128 ± 10 and 150 ± 8 Ma (Table 1 and Figure 6). The older sample, TS84, has a Dpar of 1.70 μm (Table 1 and Figures S1–S6). The younger sample, TS27, was prepared with slightly different etching conditions; therefore Dpar was not measured. The samples yielded similar track length data of 12.50 and 12.82 μm, respectively. The two samples lie on a cooling trend representing an exhumed PAZ; assuming that the two samples have similar

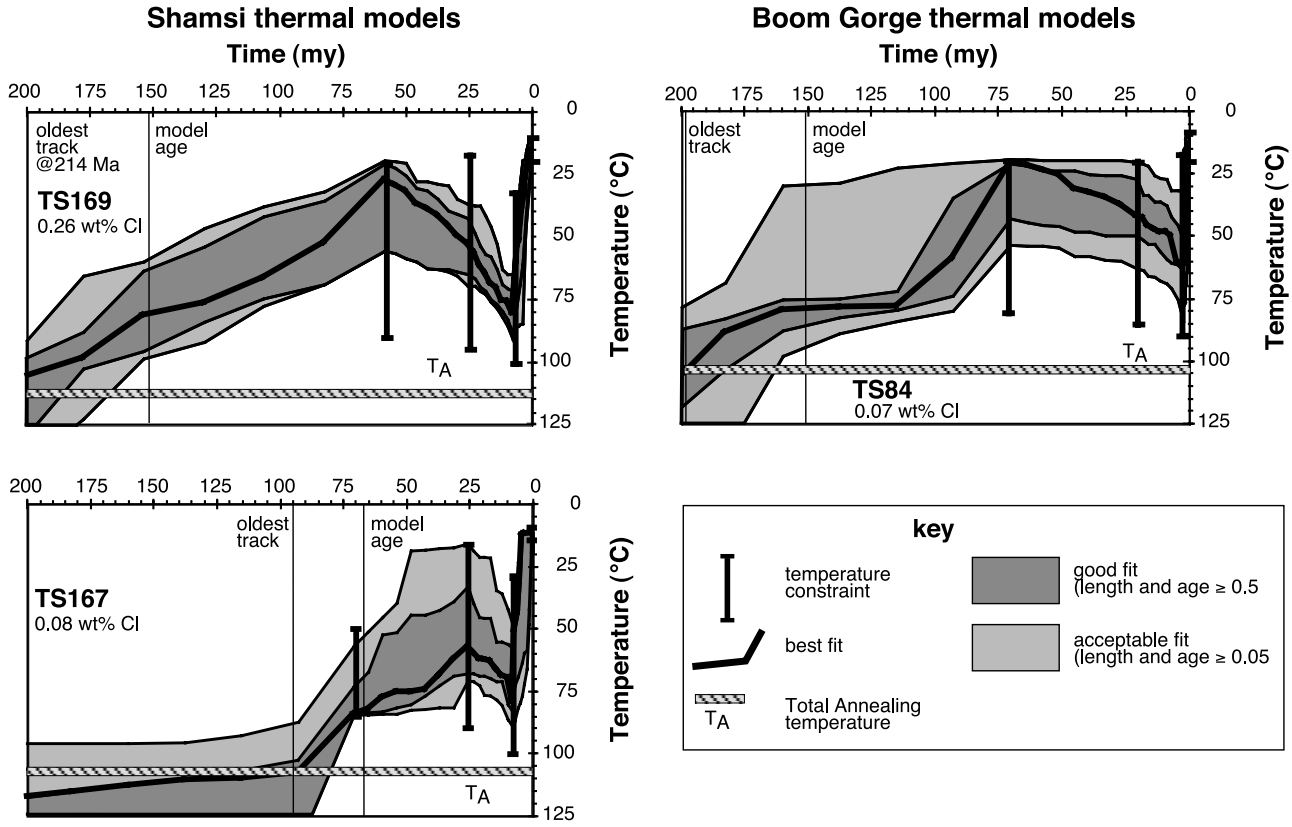

Figure 7. Representative track length models for the Shamsi and Boom Gorge profiles. See text for modeling details. Boom Gorge sample modeled using 0.07 wt % Cl, chosen by comparison with other samples to be equivalent to Dpar of 1.70 μm.

kinetic characteristics, the slope of this line is 0.01 km/Myr. Because sample TS27 is not reset even though it was collected from a structurally deep position within the Boom Gorge, the amount of exhumation in the gorge is clearly limited.

5.4. Thermal Modeling

[27] Track length modeling cannot determine a unique thermal history; rather, it yields a range of solutions that are consistent with the observed data. Thermal modeling combining track length, single crystal ages and weight percent chlorine were performed using the AFTSolve program [*Ketcham et al.*, 2000] and the annealing model of *Ketcham et al.* [1999]. This program calculates a suite of synthetic fission track data using a Monte Carlo approach and then compares the models with observed data, determining the best fit models as well as good and acceptable fits. Modeling of partially annealed samples provides good constraints on the total annealing temperature and the maximum Miocene burial temperature; the minimum temperature prior to Late Cenozoic burial is less well constrained. With information on the thermal state of the crust, this information delineates the depth of the sample below the regional erosion surface and the Late Cenozoic sediments that formerly overlay the area. Borehole data suggest that the geothermal gradient within the study area is presently 25–30°C/km [*Gubin*, 1986]; herein, we use a value of 26°C [*Shvartzman*, 1992]. The constraints on the time of final exhumation of partially annealed samples from modeling are often less precise; however, this information may be available from lower elevation samples in the same transect.

[28] Exhumation rates are more difficult to calculate, given that one must also consider advection of isotherms due to thrusting [e.g., *Brown and Summerfield*, 1997; *Mancktelow and Grasemann*, 1997] and perturbations of isotherms due to topographic effects [e.g., *Stüwe et al.*, 1994]. In this study, neither factor likely had a significant effect, because there was almost no relief when exhumation began and there were only a few kilometers of rapid exhumation. As will be shown below, significant relief likely developed after the main phase of rapid exhumation had already set the fission track ages. Apparent exhumation rates in this study are primarily between 0.2 and 1.0 mm/yr; real exhumation rates up to 1 mm/yr are associated with errors in apparent exhumation rates that are too small to be geologically meaningful [*Mancktelow and Grasemann*, 1997]. This suggests that corrections to our apparent exhumation rates are not warranted.

[29] Two of the Shamsi samples, TS167 and TS169, yielded sufficient track length measurements to permit robust thermal modeling (Figure 7); however, given that TS169 yielded twice as many measurements, these results are considered more reliable. Both samples were modeled using five time-temperature constraints. Models were started at 250 Ma, with a temperature range between 70

Table 2. Summary of AFTSolve Model Results[a]

	TS169		TS167	
	Minimum	Maximum	Minimum	Maximum
T_a, °C	112	116	106	109
T_{min}, pre-Cz sediments, °C	33	56		
T_{min}, pre-N sediments, °C			50	58
T_{max}, beneath Cz sediments, °C	79	85	79	80
Burial beneath Cz sediments, km	0.7	1.7		
Burial beneath N sediments, km			0.8	1.1
Weight percent Cl		0.26		0.08

[a]Data are summarized from all model runs that yielded good fits to the observed data. Cz is Cenozoic; N is Neogene.

and 160°C, such that all tracks initially formed could be completely annealed. The geological history requires the rock column to have cooled by the latest Cretaceous, when the Kokturpak formation was deposited above the erosion surface. Therefore a constraint was set at 70 Ma with temperature between 30°C or 50°C and 60°C or 85°C for TS169 and TS167, respectively, consistent with the samples being close to the paleosurface. The observed shortened track length distributions require a late stage heating event, consistent with additional burial heating due to the Oligo-Miocene depositional history discussed above. Three runs were made for each sample, with modeled reheating started at 30, 25, or 20 Ma. At this time, the model permitted sample temperatures between 25°C and 90°C. The peak reheating age of 7 Ma was set to match results from the vertical profile. The maximum reheating temperature was constrained to be between 30°C and 100°C. The final constraint was the present surface temperature of 10–20°C. Acceptable fits were not limited by the temperature or the position of the constraints, with the exception of the age of maximum reheating and the upper temperature limit of the 70 Ma constraint for TS167. Temperature paths between adjacent constraints had eight segments. Heating and cooling rates were not constrained. Each model run had 10,000 iterations.

[30] Several conclusions can be drawn from the modeling data (Figure 7 and Table 2). Details of the Mesozoic cooling path cannot be resolved. It is possible that the crustal column did not cool monotonically between the 250 and 70 Ma constraints that were applied; however, no independent geological data suggests that burial heating occurred during this interval. If such heating occurred, it would have caused track length reduction; in turn, this would imply that cooling occurred earlier. The influence of the Cenozoic sedimentary burial is significant; numerous model runs (not shown) which neglect this reheating did not produce good fits. The amount of heating due to burial beneath the Kokturpak formation is smaller (and less well constrained) than due to the Miocene burial. Indeed, models for TS167 cool rather than heat during deposition of the Kokturpak formation and then have a sharp heating pulse corresponding to deposition of Miocene strata. The total annealing temperature (T_a) depends on both apatite kinetic characteristics and cooling rate. T_a can be estimated as the best fit temperature at which the oldest preserved track formed; the modeled temperatures can be verified by comparison with calculated temperatures reported by *Ketcham et al.* [1999]. Results from shallow samples can be used to understand the behavior of structurally deeper samples with similar kinetic characteristics because the temperature at the depth where the inflection point in the PAZ curve formed was approximately T_a. This position would have been buried beneath a column of bedrock and the Cenozoic sedimentary basin.

[31] The amount of Cenozoic reheating experienced by the samples provides a measure of the thickness of the Late Cretaceous–Paleogene and Oligocene-Miocene sedimentary basin deposited prior to the onset of uplift of the Kyrgyz Range. From this reheating history, the thickness of the exhumed bedrock section and hence the depth of the pre-Cenozoic unconformity surface can be estimated. Assuming a geothermal gradient of 26°C/km and based on the range of modeled heating of 17–44°C (Table 2) between 0.7 and 1.7 km of sediment was deposited at Shamsi. The broad range of thicknesses is partially due to the reduced sensitivity of the model at the low temperatures experienced prior to burial. Therefore a more robust calculation taking into account the unsteady thermal conditions within a young sedimentary basin is inappropriate. However, the sedimentary thickness calculated is in agreement with geological observations from the Chu basin [*Chediya*, 1986; *Bullen et al.*, 2003].

[32] AFTSolve modeling of sample TS84 from the Boom Gorge cannot precisely constrain the timing of final exhumation (Figure 7). The modeling strategy was similar to that used with the Shamsi samples, except that reheating began at 10, 15 or 20 Ma and final cooling began at 2, 3 or 5 Ma. Best fit models suggests 2–36°C and 13–45°C of Neogene and Cenozoic heating related to burial, respectively, consistent with the up to 1.5 km of sediment preserved nearby.

6. Discussion

6.1. Multicompositional Age-Elevation Plots

[33] Kinetically similar age-elevation curves at Shamsi and Issyk Ata represent an exhumed PAZ and are expected to have similar slopes, consistent with geological data that suggests that they have experienced similar thermal histories. However, curves within the same transect representing apatites with different resistances to annealing are often not parallel because both the T_a and the influence of Cenozoic burial heating are different. For instance, a more resistant apatite is reset at a lower elevation (higher temperature); at intermediate elevations, this apatite will display an older age than less resistant apatite because the former has experienced less annealing in the (now exhumed) PAZ (Figure 5a). In the case of a single large exhumation event, more resistant apatites should lie on a steeper trend within the PAZ. However, subsequent reheating due to burial beneath a sedimentary basin can partially reset this exhumed PAZ, creating a zone with a parallel trend (Figure 5c). Subsequent exhumation can expose this history (Figure 5d). In such a case, the transition from parallel to convergent paths in the exhumed PAZ marks the base of older exhumed PAZ. At

Shamsi, this transition occurs 1 km above the base of the ultimate exhumed PAZ (Figure 6). Making the simplifying assumptions that isotherms have not been perturbed and that the geothermal gradient has remained constant, and with independent information on the amount of burial, it is possible to estimate the magnitude of the older exhumation event (compare Figure 5d). If burial beneath the Chu basin was 1 to 1.5 km, this suggests that the magnitude of the exhumation event associated with exposure of the Cretaceous surface was 2 to 2.5 km. The range of old ages obtained from the Kyrgyz range and the adjacent Chu basin [this study; *Bullen et al.*, 2001] also implies that the penultimate exhumation event was not large enough to bring more thermally resistant apatites from below the T_a to the surface.

6.2. Three-Stage Cooling History

[34] Variable age-elevation slopes for kinetically dissimilar apatites support Paleogene-Miocene burial followed by a three-stage cooling history for the Kyrgyz Range: (1) rapid cooling during removal of Cenozoic cover strata, (2) initially reduced erosion and cooling following exhumation of pre-Cenozoic bedrock, and (3) renewed rapid cooling and erosion into bedrock (Figure 8). This history is best defined by the Shamsi age-elevation curve. Only the lower portion of the Issyk Ata curve can presently be well defined with this cooling history. Although erosion has partially removed the AFT record of three-stage cooling at Ala Archa, it is also defined by U-Th/He dating of apatite there [*Bullen et al.*, 2003].

[35] For Issyk Ata and Shamsi, the portion of the age-elevation plot below the inflection point yields apparent exhumation rates of 0.3 ± 0.1 and $\sim$1 km/Myr, respectively. The $\sim$1 to 1.5 km of sediment overlying the basement would require between 2 and 7 Myr and 1 and 1.5 Myr, respectively, to have been removed at these rates. For Shamsi, where the age and paleodepth of the inflection point is moderately well constrained as 7 ± 2 Ma and 4.0 to 4.6 km (Figure 6), the mean exhumation rate from this point to the surface is 0.4 to 0.9 km/Myr. This suggests that the rapid cooling recorded in the age-elevation profiles reflects the removal of the sedimentary section and that the exhumation rate decreased at least slightly afterward. Similar conclusions about the magnitude of exhumation were reached by *Bullen et al.* [2003] for the Ala Archa section, based on both apatite fission track and U-Th/He thermochronology. In particular, these authors concluded that a $\sim$1 Myr pulse of rapid exhumation at circa 11–10 Ma removed 1.5 km of section at 1.0–1.5 km/Myr. Subsequently, the exhumation rate decreased to <0.3 km/Myr until 3 Ma, when the rate increased again to 0.8 km/Myr. These changes were similar in magnitude to synchronous changes in rates of shortening along the northern flank of the central Kyrgyz Range and rates of sediment accumulation in the Chu Basin [*Bullen et al.*, 2003]. The fission track data presented in this study cannot address whether the exhumation rate changed in the last several million years at Issyk Ata or Shamsi.

[36] The three-stage cooling pattern documented in the Kyrgyz range is likely to be broadly applicable. The typical geometry of a foreland-propagating thrust belt includes a foreland basin that is eventually disrupted by the advancing reverse fault front (Figure 8). In this setting, uplift above a new thrust or fold first exhumes the recently deposited sediment of the foreland basin. These sediments are typically poorly cemented and therefore easily eroded. Only when the vertical displacement of the fault exceeds the thickness of the overlying young sediment are older units exposed. Easily eroded, recently deposited sedimentary rocks can be rapidly exhumed with negligible surface uplift. For example, nearby active fault-cored folds in Cenozoic strata maintain less than 200 m of topographic relief despite relative rock uplift rates of over 1 mm/yr [*Thompson et al.*, 2002]. As increasing amounts of resistant basement are exposed, exhumation rates decrease while surface uplift rates increase, if shortening rates remain steady [cf. *Burbank et al.*, 1999; *Sobel and Strecker*, 2003]. Surface processes immediately respond to topographic relief developed by range growth and initiate drainage networks that can eventually bring erosion rates into balance with rock uplift rates. Orographically enhanced precipitation and glacial erosion may further enhance the effectiveness of erosion as the range grows. At this point, if the timescale of geomorphic

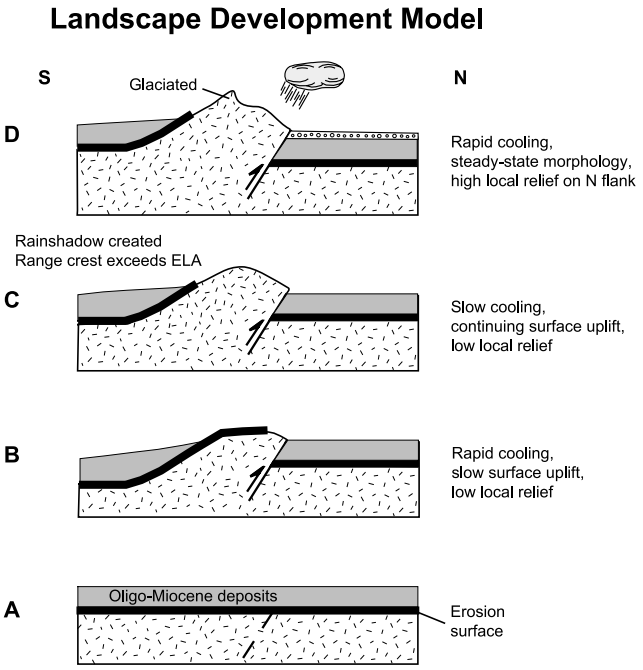

Figure 8. Schematic evolution of topography in the Kyrgyz range, showing the effect of contrasting lithologies on exhumation and surface uplift rates. (a) Oligocene–early Miocene foreland basin deposited above regional erosion surface. (b) Rapid exhumation of sediments in hanging wall of thrust causing rapid cooling but slow surface uplift of range. (c) Area of exposed basement increasing relative to young sedimentary cover, and erosion rates decreasing, leading to increasing surface uplift rates. (d) Range becoming large enough to create a significant orographic barrier; subsequently placing upper portion of range above equilibrium line altitude (ELA). Glacial erosion causes drainage basins on windward side to expand at the expense of more arid, less deeply incised basins on the leeward side.

adjustment to range uplift is sufficiently rapid, range morphology may reach a steady state dictated by the interplay of surface processes and rock uplift.

6.3. Lateral Propagation Rate

[37] The transition from slow cooling, followed by burial, to rapid cooling measures exhumation of the Kyrgyz Range via initial erosional stripping of Cenozoic cover strata at the onset of thrusting at the range tip. The best estimates for the onset of this rapid exhumation are 11 ± 0.5 Ma at Ala Archa [*Bullen et al.*, 2001] and 7 ± 2 Ma at Shamsi; these sections are 64 ± 7 km apart (Figure 6). The start of exhumation at Issyk Ata, located halfway between these locations, can only be constrained as slightly older than 8 Ma. Plotting the age that rapid cooling initiated versus distance east of Ala Archa shows that the range has propagated eastward at ~16 km/Myr from 11 ± 0.5 to 7 ± 2 Ma. Given the uncertainties in the ages, permissible rates range from as low as 10 km/Myr to as high as 42 km/Myr. The lower range is consistent with quasi-constant eastward propagation rates from Ala Archa all the way to the Boom Gorge; the higher range requires dramatically diminished rates in the Late Miocene. If the propagation rate is constant then fault slip rates must diminish after initiation in order to explain the form of surface uplift at the easternmost end of the range.

[38] Progressive changes in the geomorphology of basement rocks that form the easternmost Kyrgyz Range provides some independent constraint as to the relative rates of lateral propagation and uplift. As soon as rock uplift raises the Cenozoic sedimentary cover rocks above local base level, they appear to be rapidly stripped from above the pre-Cenozoic erosion surface and do not contribute significantly to the topography of the range [*Burbank et al.*, 1999]. Topographic relief grows primarily within the pre-Cenozoic bedrock via surface uplift that results from the competition between rock uplift and exhumation. The abrupt increases in mean and maximum elevation in the surface uplift zone (Figure 4) suggests that the form of the nascent range near its terminus is dictated primarily by rock uplift above the south dipping thrust fault, that peak heights are correlated with the magnitude of fault slip, and that the magnitude of dissection is minimal. The east-west gradient of peak elevations in the surface uplift zone define a slope of 13% ± 2% (Figure 4). If this gradient is built by a laterally propagating thrust fault with spatially uniform slip along it following initiation at any given site, and if no significant erosion of the peaks occurs, the preserved geometric slope of the range crest implies that the lateral propagation rate is only 7 to 9 times the rock uplift rate. Such a gradient could not have applied over the entire interval of range growth because it would require over 15 km of rock uplift in the central part of the range; this amount is inconsistent with the fission track data from Ala Archa where total rock uplift is estimated to be 6.5 km [*Bullen et al.*, 2003]. Hence the propagation/rock uplift ratio appears considerably lower near the eastern tip of the range than it does farther west. An elliptical distribution of fault slip, similar to that documented for propagating normal faults [*Dawers et al.*, 1993], could be responsible for a steeper rock uplift gradient on the presently propagating easternmost tip of the Kyrgyz Range than that derived from Miocene exhumation of the central part of the range. Alternatively, a diminished lateral propagation rate could have arisen in response to structural interference [*Gupta and Scholz*, 2000] with reverse faults and strike-slip faults that emerge from the Kungey Alatoo to the northeast. Independent geochronological constraints of either fault slip rate or the ages of initiation of glaciation in the easternmost Kyrgyz Range as rocks were uplifted above the glacial ELA could test these predictions.

6.4. Geomorphic Adjustment to Bedrock Uplift

[39] The geomorphic evolution of the Kyrgyz Range supports progressive adjustment of surface uplift and incision in response to rock uplift. At the easternmost propagating tip of the Kyrgyz Range, limited dissection of the pre-Cenozoic erosion surface enhances surface uplift and dampens development of relief. This contrasts with the steady morphology zone in the central part of the range (Figure 4) where the pre-Cenozoic erosion surface has been completely removed and large north facing basins predominate. In between these zones, the transition zone provides important insight into the transformation of the Kyrgyz Range by surface processes. Peak heights increase gradually from east to west within the transition zone, albeit at a much more gentle gradient than in the surface uplift zone, because of greater competition between rock uplift and erosion. The most striking aspect of the transition zone is that mean elevation attains a near-constant value of ~3200 m despite ongoing growth of both peak heights and the range of hypsometry (Figure 4). Systematic increase of north facing basin size explains these contradictory elevation and relief trends. The first significant enlargement of north facing basins occurs where peak elevations exceed 3500 m elevation above mean sea level (Figure 4), enabling Pleistocene glaciation of the range crest to lengthen north facing basins southward via cirque retreat (Figure 3), [*Oskin and Burbank*, 2005]. Hypsometry remains concentrated near the glacial ELA within these glacially expanded north facing catchments because glacial erosion is limited to high elevations. [cf. *Brozovic et al.*, 1997]. Farther west within the transition zone, expansion of north facing basins eventually leads to more effective fluvial and glacial erosion at lower elevations, which in turn causes the range of hypsometry to expand. In the westernmost transition zone, the range of hypsometry attains its maximum as rivers in deeply incised valleys abut against hillslopes that are at or near the threshold angle for failure. Overall, the transition zone appears to be a region of stabilization of elevation, if not locally even of surface depression, as large north facing basins enlarge and mature.

6.5. Coupled Exhumation and Shortening

[40] Structural reconstructions of the central Kyrgyz Range [*Bullen et al.*, 2003] suggest that the pattern of shortening may be correlated to the exhumation rate. Initial, rapid shortening above a reverse fault corresponds to high cooling rates during removal of Cenozoic cover rocks from the crest of the range. This was followed by a period of slow shortening rate and backthrusting within the foreland basin,

north of the Kyrgyz Range, corresponding to a period of slow exhumation of Paleozoic bedrock. In the past 3 Myr, both shortening rate and exhumation of the bedrock core have increased. If the exhumation history of the Kyrgyz Range is driven by the interplay of rock erodability with both rock and surface uplift, then this correlation could indicate a feedback mechanism whereby exhumation rates are reduced when more resistant rocks are at the surface, thereby building topography. To the extent that larger topographic loads require more work for a given increment of shortening and rock uplift, shortening and both rock and surface uplift rates may diminish as topography grows and the locus of deformation shifts elsewhere in the range [e.g., *Masek and Duncan*, 1998]. If erosion in a given range is inefficient and its topography grows, the increased load may cause shortening rates to diminish or deformation to shift entirely to a site requiring less work. This model predicts temporal variations in exhumation rate that are driven by changes in erosion parameters; the evidence of this behavior should be detectable both in the cooling history of the range and in the depositional history of the adjacent basin. If the Kyrgyz Range has continued to evolve in a similar manner to that expressed in the bedrock and detrital cooling history [*Bullen et al.*, 2003], then the along-strike geomorphic evolution of the range should also be consistent with the proposed exhumation model. Here we explore the plausibility of coupling between surface uplift and shortening rate at the range scale.

[41] In the Kyrgyz Range, following a long Cenozoic interval of tectonic quiescence and deposition, a short pulse of rapid cooling at several sites is associated with 1 to 1.5 km of exhumation; this thickness corresponds well with the thickness of the young sedimentary basin which formerly overlay the range. Therefore most of this pulse of rapid cooling is probably attributable to the removal of this sediment during the initial phase of rock uplift. Because the young sedimentary rocks are more easily eroded than the underlying Paleozoic units, this short episode of rapid cooling likely corresponded to only a small amount of surface uplift [*Bullen et al.*, 2003]. Only when a significant amount of bedrock was exposed could the surface uplift increase and the concurrent exhumation rate decrease. This pattern is seen in the geomorphology of the surface uplift zone of the Kyrgyz Range, where easily eroded Cenozoic rocks are rapidly removed from the range but the underlying pre-Cenozoic unconformity surface is widely preserved up to high elevations. The observation that an initial pulse of rapid exhumation propagates along the strike of the range, roughly normal to the principal shortening direction, suggests that the range is growing due to lengthening of the bounding structure rather than due to changes in the regional stress field.

[42] On the basis of structural and thermochronologic data in the central Kyrgyz Range near Ala Archa, *Bullen et al.* [2003] suggested that the decrease in exhumation rate at circa 10 Ma was associated with the observed decrease in range-normal shortening rate and with a shift from thrusting to backthrusting. We further suggest that as the range-bounding thrust fault lengthened, this deformation pattern likely propagated along the strike of the range in the same manner. Basinward propagating foreland thrust faults and folds, including prominent backthrusts, are observed along the length of the range east from Ala Archa. We deduce from the thermal history of lateral range propagation that these foreland faults have also propagated eastward as the range itself propagated. Such a spatially varying decrease in shortening rate, if supported from the history of these foreland structures, would suggest a feedback between the size of the range and the activity of the basal thrust and growing topography [cf. *Davis et al.*, 1983].

6.6. Steady State Timescale

[43] Consistency between the cooling history and the along-strike geomorphic evolution of the Kyrgyz Range supports the hypothesis that exhumation rate, and possibly also shortening rate, are modulated by the timescale of adjustment of surface processes to rock uplift. No single steady state timescale adequately describes the variety and significance of adjustments toward steady morphology in the Kyrgyz Range. Erosion is immediately effective at stripping the Cenozoic sedimentary cover from the pre-Cenozoic erosion surface, supporting an initial, short adjustment time of less than 1 Myr for steady state rock uplift and erosion of Cenozoic strata. Conversely, significantly longer time periods are necessary for erosion to balance rock uplift of resistant Paleozoic basement. In the surface uplift zone, below the elevation of glacial ice accumulation, surface processes fail to substantively alter the structural form of the range. Nonglaciated ranges in the western Tien Shan with summits over 3500 m elevation and with as much as 2000 m of relief commonly preserve extensive areas of the pre-Cenozoic erosion surface [*Burbank et al.*, 1999]. Glaciation of the easternmost Kyrgyz Range triggers the first significant erosional response to rock uplift via establishing, lengthening, and incising canyons [*Oskin and Burbank*, 2005]. Formation of relief here corresponds to a sharp decrease in mean basin hypsometry and increasing mean hillslope angles as glacio-fluvial erosion counterbalances, and even temporarily exceeds, rock uplift. Over 80% of the adjustment of hypsometry, peak elevations and mean slope angles occurs within the first 25 km of the transition zone, suggesting that a quasi-steady state is reached within 2–3 Myr after the onset of glaciation and canyon cutting in the surface uplift zone. The complete transition to a steady morphology occurs gradually and cannot be defined by a sharp break in morphometric indices at the end of the transition zone. Mean hypsometry is steady between 3000 and 3500 m for all points west of the surface uplift zone. Mean slope angle levels off gradually west of Shamsi, and the range of hypsometry climbs to maximum values west of Issyk Ata. Overall, approximately 110 km of the east Kyrgyz Range shows evidence for dynamic adjustment of its geomorphology to balance erosion and rock uplift. This probably represents over 10 Myr of range propagation, and suggests that the timescale of geomorphic adjustment over active basement-cored uplifts of the Tien Shan spans back into Late Miocene time – representing most of the total Cenozoic contractile history of the northern Tien Shan.

[44] In actively deforming mountain ranges, the time to steady state is likely to be dependent on the efficiency of surface processes and the rates of deformation. Rapid rock uplift rates tend to generate steep hillslopes and rivers, thereby accelerating erosion rates. Numerical models suggest that topographic steady state can be attained in <1 Myr where rates of deformation and erosion are high (equivalent to several millimeters per year [*Willett*, 1999]). Not surprisingly, in the Kyrgyz Range where rates are commonly $\leq$1 mm/yr, a longer interval is expected to be required to attain steady state.

7. Conclusions

[45] Apatite fission track data from the Kyrgyz Range document the lateral growth of the range. This is one of the first studies to use multiple vertical AFT profiles along the trend of a single structure to constrain the location and geometry of a warped PAZ, thereby documenting the magnitude of differential exhumation along strike. The PAZ has a relief of at least 500 m between the three hanging wall profiles. In the Boom Gorge footwall profile, the PAZ lies about 2500 m lower than the adjacent Shamsi hanging wall profile, implying that the fault has roughly this amount of offset.

[46] Comparisons between exhumation histories derived from apatite fission track analysis and the geomorphic evolution based on quantitative DEM analysis of the Kyrgyz Range permits a reconstruction of the entire Neogene evolution of the range. Following extended tectonic quiescence and deposition within the foreland, exhumation of the range commenced at circa 11 Ma in the central Kyrgyz Range in the vicinity of Ala Archa and has subsequently propagated eastward. The lateral propagation rate between Ala Archa and Shamsi was $\sim 16^{+26}_{-6}$ km/Myr from 11 ± 0.5 Ma to 7 ± 2 Ma; this rate likely slowed as the range propagated farther eastward toward the Kungey Alatoo. Initial rock uplift led to rapid stripping of poorly consolidated, Cenozoic sedimentary rocks. Such rapid exhumation may have (almost) balanced rock uplift, creating only limited surface uplift. The $\sim$1.5-km-thick portion of the Chu basin which formerly overlay the range above the Cretaceous erosion surface was stripped away in 1–2 Myr, corresponding to the brief episode of rapid cooling documented by apatite fission track analysis. Therefore as the range grows, this zone of rapid sediment removal propagates along strike. Once significant amounts of more resistant basement were exposed, the exhumation rate would be expected to have decreased while the surface uplift rate would increase if range-normal shortening rates were maintained. However, independent data suggest that the shortening rate actually decreased, supporting a possible feedback between erosional efficiency and the location and magnitude of shortening. As resistant basement rocks were uplifted and topographic relief increased, drainage networks propagated into the growing range, eventually bringing erosion rates into balance with rock uplift rates. The timescale for the majority of this geomorphic adjustment is $\sim$2 to 3 Myr after the range crest was uplifted through the glacial ELA and the subsequent development of glacially lengthened and incised canyons. However, additional systematic adjustments to mean slope angle and hypsometry occurred before the transition to steady morphology was complete. Overall, the evolution of the Kyrgyz Range supports a model of a systematically time-varying exhumation and shortening rates that are modulated by changes in rock erodability, the efficiency of erosion processes, and the timescale of geomorphic adjustment to surface uplift.

[47] **Acknowledgments.** Dieter Rhede and Oona Appelt helped collect the electron microprobe data. Mike Bullen kindly provided unpublished apatite kinetic data from the Ala Archa section. A.M. acknowledges support from the DAAD. Partial funding was provided by NASA (NAG5-9039; 10520). Nick Arnaud provided useful advice about error calculations. The manuscript benefited from helpful reviews by Andy Carter, Laurent Bollinger, and Eric Kirby.

References

Abbott, L. D., E. A. Silver, R. S. Anderson, R. B. Smith, J. C. Ingle, S. A. Kling, D. Haig, E. Small, J. Galewsky, and W. Sliter (1997), Measurement of the tectonic uplift rate in a young collisional mountain belt, Finisterre Range, Papua New Guinea, *Nature*, *385*, 501–507.

Abdrakhmatov, K. E., R. Weldon, S. Thompson, D. Burbank, C. Rubin, M. Miller, and P. Molnar (2001), Origin, direction, and rate of modern compression in the central Tien Shan, Kyrgyzstan (in Russian), *Geol. Geofiz.*, *42*, 1585–1609.

Abdrakhmatov, K. Y., et al. (1996), Relatively recent construction of the Tien Shan inferred from GPS measurements of present-day crustal deformation rates, *Nature*, *384*, 450–453.

Ahnert, F. (1970), Functional relationships between denudation, relief, and uplift in large mid-latitude basins, *Am. J. Sci.*, *268*, 243–263.

Aizen, V. B., E. M. Aizen, and J. M. Melack (1995), Climate, snow cover, glaciers, and runoff in the Tien Shan, Central Asia, *Water Resour. Bull.*, *31*(6), 1113–1129.

Bazhenov, M. L., V. S. Burtman, and A. V. Dvorova (1999), Permian paleomagnetism of the Tien Shan fold belt, central Asia: Post-collisional rotations and deformation, *Tectonophysics*, *312*, 303–329.

Bazhenov, M. L., A. Q. Collins, K. E. Degtyarev, N. M. Levashova, A. V. Mikolaichuk, V. E. Pavlov, and R. Van der Voo (2003), Paleozoic northward drift of the North Tien Shan (central Asia) as revealed by Ordovician and Carboniferous paleomagnetism, *Tectonophysics*, *366*, 113–141.

Brown, R. W., and M. A. Summerfield (1997), Some uncertainties in the derivation of rates of denudation from thermochronologic data, *Earth Surf. Processes Landforms*, *22*(3), 239–248.

Brozovic, N., D. W. Burbank, and A. J. Meigs (1997), Climatic limits on landscape development in the northwestern Himalaya, *Science*, *276*, 571–574.

Bullen, M. E., D. W. Burbank, J. I. Garver, and K. Y. Abdrakhmatov (2001), Late Cenozoic tectonic evolution of the northwestern Tien Shan: New age estimates for the initiation of mountain building, *Geol. Soc. Am. Bull.*, *113*, 1544–1559.

Bullen, M. E., D. W. Burbank, and J. I. Garver (2003), Building the northern Tien Shan: Integrated thermal, structural, and topographic constraints, *J. Geol.*, *111*(2), 149–165.

Bune, V. I., and G. P. Gorshkov (1980), *Seismic Zoning Territory of the USSR. Methodical Bases and the Regional Description of the Map of 1978 Year* (in Russian), 306 pp., Nauka, Moscow.

Burbank, D., A. Meigs, and N. Brozovic (1996), Interactions of growing folds and coeval depositional systems, *Basin Res.*, *8*, 199–223.

Burbank, D. W., J. K. McLean, M. Bullen, K. Y. Abdrakhmatov, and M. M. Miller (1999), Partitioning of intermontane basins by thrust-related folding, Tien Shan, Kyrgyzstan, *Basin Res.*, *11*(1), 75–92.

Burg, J.-P., A. V. Mikolaichuk, and F. C. Apayarov (Eds.) (2004), Digital geological map of the Kyrgyz Range and Chu Basin transitional zone, SNF, Project 7KSPJ065518, ETH-Zurich, Zurich. (Available at http://www.kyrgyzstan.ethz.ch/)

Burtman, V. S. (1975), Structural geology of Variscan Tien Shan, USSR, *Am. J. Sci.*, *275–A*, 157–186.

Carroll, A. R., S. A. Graham, E. Chang, and C. L. McKnight (2001), Sinian through Permian tectonostratigraphic evolution of the northwestern Tarim basin, China, in *Paleozoic and Mesozoic Tectonic Evolution of Central and Eastern Asia: From Continental Assembly to Intracontinental Deformation*, edited by M. S. Hendrix and G. A. Davis, *Mem. Geol. Soc. Am.*, *194*, 47–70.

Cartwright, J. A., B. D. Trudgill, and C. S. Manfeld (1995), Fault growth by segment linkage: An explanation for scatter in maximum displacement and trace length data from the Canyonlands grabens of SE Utah, *J. Struct. Geol.*, *17*, 1319–1326.

Chediya, O. K. (1986), *Morfostruktury i noveishii tektogenez Tyan'-Shanya (Morfostructures and Neotectonics of the Tien Shan)*, 314 pp., Ilim, Frunze, Kyrgyzstan.

Chediya, O. K., V. M. Yazovskii, and A. B. Fortuna (1973), O stratigraficheskom raschlenenii krasnotsvetnogo kompleksa v Chuyskoy vpadine I yeye gornom obramlenii (The stratigraphic subdivision of the Kyrgyz red-bed complex in the Chu basin and the surrounding mountains), in *Zakonomernosti Geologicheskogo Razvitiya Tyan-Shanya v Kaynozoye (Principles of the Geologic Development of the Tyan-Shan in the Cenozoic)*, pp. 26–52, Ilim, Bishkek, Kyrgyzstan.

Chediya, O. K., K. Y. Abdrakhmatov, I. H. Lamzin, G. Michel, and V. Michailev (1998), Seismotectonic characterization of the Issyk Ata fault, report, pp. 58–69, Inst. Nauk Kyrgyzskoi, Bishkek, Kyrgyzstan.

Cobbold, P. R., E. Sadybakasov, and J. C. Thomas (1996), Cenozoic transpression and basin development, Kyrgyz Tien Shan, central Asia, in *Geodynamic Evolution of Sedimentary Basins*, edited by F. Roure et al., pp. 181–202, Technip, Paris.

Crowhurst, P. V., P. F. Green, and P. J. J. Kamp (2002), Appraisal of (U-Th)/He apatite thermochronology as a thermal history tool for hydrocarbon exploration: An example from the Taranaki Basin, New Zealand, *AAPG Bull.*, *86*(10), 1801–1819.

Davis, D., J. Suppe, and F. A. Dahlen (1983), Mechanics of fold-and-thrust belts and accretionary wedges, *J. Geophys. Res.*, *88*, 1153–1172.

Davis, K., D. W. Burbank, D. Fisher, S. Wallace, and D. Nobes (2005), Thrust-fault growth and segment linkage in the active Ostler fault zone, New Zealand, *J. Struct. Geol.*, *27*, 1528–1546.

Dawers, N. H., M. H. Anders, and C. H. Scholz (1993), Growth of normal faults: Displacement-length scaling, *Geology*, *21*, 1107–1110.

Donelick, R. A., R. A. Ketcham, and W. D. Carlson (1999), Variability of apatite fission-track annealing kinetics: II. Crystallographic orientation effects, *Am. Mineral.*, *84*(9), 1224–1234.

Dumitru, T. A. (1993), A new computer automated microscope stage system for fission track analysis, *Nucl. Tracks*, *21*(4), 575–580.

Dumitru, T. A., D. Zhou, E. Z. Chang, S. A. Graham, M. S. Hendrix, E. R. Sobel, and A. R. Carroll (2001), Uplift, exhumation, and deformation in the Chinese Tian Shan, in *Paleozoic and Mesozoic Tectonic Evolution of Central and Eastern Asia: From Continental Assembly to Intracontinental Deformation*, edited by M. S. Hendrix and G. A. Davis, *Mem. Geol. Soc. Am.*, *194*, 71–99.

England, P. C., and P. Molnar (1990), Surface uplift, uplift of rocks, and exhumation of rocks, *Geology*, *18*(12), 1173–1177.

Erslev, E. A. (1986), Basement balancing of Rocky Mountain foreland uplifts, *Geology*, *14*, 259–262.

Fitzgerald, P. G., R. B. Sorkhabi, T. F. Redfield, and E. Stump (1995), Uplift and denudation of the central Alaska Range: A case study in the use of apatite fission track thermochronology to determine absolute uplift parameters, *J. Geophys. Res.*, *100*, 20,175–20,191.

Fortuna, A. B., C. K. Kerimbekov, S. I. Kyzikov, and A. V. Mikolaichuk (1994), Lithostratigraphic and palynologic data of Cenozoic deposits of Tessik–Sarybulak depression, in *Geology of Cenozoic and Seismotectonics of the Tien Shan*, pp. 26–39, Ilim, Bishkek, Kyrgyzstan.

Galbraith, R. F. (1981), On statistical models for fission track counts, *Math. Geol.*, *13*, 471–478.

Green, P. F. (1981), A new look at statistics in fission-track dating, *Nucl. Tracks*, *5*, 77–86.

Green, P. F., I. R. Duddy, A. J. W. Gleadow, and J. F. Lovering (1989a), Apatite fission-track analysis as a paleotemperature indicator for hydrocarbon exploration, in *Thermal History of Sedimentary Basins: Methods and Case Histories*, edited by N. D. Naeser and T. H. McCulloh, pp. 181–195, Springer, New York.

Green, P. F., I. R. Duddy, G. M. Laslett, K. A. Hegarty, A. J. W. Gleadow, and J. F. Lovering (1989b), Thermal annealing of fission tracks in apatite, 4, Quantitative modelling techniques and extension to geological timescales, *Chem. Geol.*, *79*, 155–182.

Gubin, I. E. (1986), *Lithosphere of Tien Shan*, 158 pp., Nauka, Moscow.

Gupta, A., and C. Scholz (2000), A model of normal fault interaction based on observations and theory, *J. Struct. Geol.*, *22*, 865–879.

Hallet, B., L. Hunter, and J. Bogen (1996), Rates of erosion and sediment evacuation by glaciers: A review of field data and their implications, *Global Planet. Change*, *12*, 213–235.

Hendrix, M. S., S. A. Graham, A. R. Carroll, E. R. Sobel, C. L. McKnight, B. J. Schulein, and Z. Wang (1992), Sedimentary record and climatic implications of recurrent deformation in the Tian Shan: Evidence from Mesozoic strata of the north Tarim, south Junggar, and Turpan basins, northwest China, *Geol. Soc. Am. Bull.*, *104*, 53–79.

Hendrix, M. S., T. A. Dumitru, and S. A. Graham (1994), Late Oligocene–early Miocene unroofing in the Chinese Tian Shan: An early effect of the India-Asia collision, *Geology*, *22*, 487–490.

Howard, A. D. (1994), A detachment-limited model of drainage basin evolution, *Water Resour. Res.*, *30*, 2261–2285.

Hurford, A. J., and P. F. Green (1983), The zeta age calibration of fission-track dating, *Chem. Geol.*, *41*(4), 285–317.

Ketcham, R. A., R. A. Donelick, and W. D. Carlson (1999), Variability of apatite fission-track annealing kinetics: III. Extrapolation to geological time scales, *Am. Mineral.*, *84*(9), 1235–1255.

Ketcham, R. A., R. A. Donelick, and M. B. Donelick (2000), AFTSolve: A program for multi-kinetic modeling of apatite fission-track data, *Geol. Mater. Res.*, *2*(1), 1–32.

Kooi, H., and C. Beaumont (1996), Large-scale geomorphology: Classical concepts reconciled and integrated with contemporary ideas via a surface processes model, *J. Geophys. Res.*, *101*, 3361–3386.

Krilov, A. Y. (1960), Absolute age of the rocks of the central Tien Shan and application of Argon methods to metamorphic and sedimentary sediments, in *Determination of the Absolute Age of Pre-Quaternary Formations*, edited by I. E. Starik, pp. 222–224, Nedra, Moscow.

Makarov, V. I. (1977), *New Tectonic Structure of the Central Tien Shan*, 172 pp., Nauka, Moscow.

Mancktelow, N. S., and B. Grasemann (1997), Time-dependent effects of heat advection and topography on cooling histories during erosion, *Tectonophysics*, *270*, 167–195.

Masek, J. G., and C. C. Duncan (1998), Minimum-work mountain building, *J. Geophys. Res.*, *103*, 907–917.

Mikolaichuk, A. V. (2000), The structural position of thrusts in the recent orogen of the central Tien Shan, *Russ. Geol. Geophys.*, *41*(7), 961–970.

Mikolaichuk, A., E. Sobel, M. Gubrenko, and A. Lobanchenko (2003), Structural evolution of the Tien Shan orogenic northern margin, *Proc. Natl. Acad. Sci. Kyrgyz Repub.*, *4*, 50–58.

Oskin, M., and D. W. Burbank (2005), Alpine landscape evolution dominated by cirque retreat, *Geology*, *33*, 933–936.

Reigber, C., G. W. Michel, R. Galas, D. Angermann, J. Klotz, J. Y. Chen, A. Papschev, R. Arslanov, V. E. Tzurkov, and M. C. Ishanov (2001), New space geodetic constraints on the distribution of deformation in central Asia, *Earth Planet. Sci. Lett.*, *191*(1–2), 157–165.

Schmidt, K. M., and D. R. Montgomery (1996), Rock mass strength assessment for bedrock landsliding, *Environ. Eng. Geosci.*, *2*, 325–338.

Shvartzman, Y. G. (1992), Thermal field, seismicity and geodynamics of the Tien Shan, Ph.D. dissertation thesis, Univ. of Kyrgyzstan, Bishkek.

Sklar, L. S., and W. E. Dietrich (2001), Sediment and rock strength controls on river incision into bedrock, *Geology*, *29*, 1087–1090.

Sobel, E. R. (1999), Basin analysis of the Jurassic–Lower Cretaceous southwest Tarim basin, NW China, *Geol. Soc. Am. Bull.*, *111*, 709–724.

Sobel, E. R., and T. A. Dumitru (1997), Exhumation of the margins of the western Tarim basin during the Himalayan orogeny, *J. Geophys. Res.*, *102*, 5043–5064.

Sobel, E. R., and M. R. Strecker (2003), Uplift, exhumation, and precipitation: Tectonic and climatic control of Late Cenozoic landscape evolution in the northern Sierras Pampeanas, Argentina, *Basin Res.*, *15*(4), 431–451, doi:10.1046/j.1365-2117.2003.00214.x.

Sobel, E., A. Mikolaichuk, J. Chen, and D. Burbank (2000), Development of the Late Cenozoic central Tian Shan in Kyrgyzstan and China recorded by apatite fission track thermochronology, *Eos Trans. AGU*, *81*(48), Fall Meet. Supp., Abstract T71D-03.

Sobel, E. R., G. E. Hilley, and M. R. Strecker (2003), Formation of internally drained contractional basins by aridity-limited bedrock incision, *J. Geophys. Res.*, *108*(B7), 2344, doi:10.1029/2002JB001883.

Sobel, E. R., D. Seward, G. Ruiz, A. Kuonov, H. Ege, M. Wipf, and C. Krugh (2004), Influence of etching conditions on Dpar measurements: Implications for thermal modeling, paper presented at International Conference on Fission Track and Thermochronology, Free Univ., Amsterdam, Netherlands, 8–14 Aug.

Stock, J. D., and D. R. Montgomery (1999), Geologic constraints on bedrock river incision using the stream power law, *J. Geophys. Res.*, *104*, 4983–4993.

Stüwe, K., L. White, and R. Brown (1994), The influence of eroding topography on steady-state isotherms: Application to fission track analysis, *Earth Planet. Sci. Lett.*, *124*(1–4), 63–74.

Thompson, S. C., R. J. Weldon, C. M. Rubin, K. Abdrakhmatov, P. Molnar, and G. W. Berger (2002), Late Quaternary slip rates across the central Tien Shan, Kyrgyzstan, central Asia, *J. Geophys. Res.*, *107*(B9), 2203, doi:10.1029/2001JB000596.

Trofimov, A. K., N. F. Udalov, N. G. Utkina, F. B. Fortuna, O. K. Chediya, and V. M. Yazovskii (1976), *Geologiya kainozoya Chuiskoi vpadiny i ee gornogo obramleniya (Cenozoic Geology of the Chu Depression and Its Mountainous Surroundings)*, 128 pp., Nauka, St. Petersburg, Russia.

Whipple, K. X. (2004), Bedrock rivers and the geomorphology of active orogens, *Annu. Rev. Earth Planet. Sci.*, *32*, 151–185.

Whipple, K. X., and G. E. Tucker (1999), Dynamics of the stream-power river incision model: Implications for height limits of mountain ranges, landscape response timescales, and research needs, *J. Geophys. Res.*, *104*, 17,661–17,674.

Willett, S. D. (1999), Orogeny and orography: The effects of erosion on the structure of mountain belts, *J. Geophys. Res.*, *104*, 28,957–28,981.

Willett, S. D., and M. T. Brandon (2002), On steady states in mountain belts, *Geology*, *30*(2), 175–178.

Yin, A., S. Nie, P. Craig, T. M. Harrison, F. J. Ryerson, X. L. Qian, and G. Yang (1998), Late Cenozoic tectonic evolution of the southern Chinese Tian Shan, *Tectonics*, *17*, 1–27.

Zhang, P., P. Molnar, and W. R. Downs (2001), Increased sedimentation rates and grain sizes 2–4 Myr ago due to the influence of climate change on erosion rates, *Nature*, *410*, 891–897.

D. Burbank, Department of Earth Sciences, University of California, Santa Barbara, CA 93106, USA.

A. Mikolaichuk, Institute of Geology, 30 Erkindyk Ave., Bishkek 720481, Kyrgyzstan.

M. Oskin, Department of Geological Sciences, University of North Carolina at Chapel Hill, Chapel Hill, NC 27599, USA.

E. R. Sobel, Institut fuer Geowissenschaften, Universitaet Potsdam, Postfach 601553, D-14415 Potsdam, Germany. (sobel@rz.uni-potsdam.de)